IEEE Access
Multidisciplinary | Rapid Review | Open Access Journal

Received 6 February 2023, accepted 2 March 2023, date of publication 10 March 2023, date of current version 16 March 2023.

Digital Object Identifier 10.1109/ACCESS.2023.3255417

APPLIED RESEARCH

Prognostics and Health Management of Rotating Machinery via Quantum Machine Learning

CAIO BEZERRA SOUTO MAIOR[1,2], LAVÍNIA MARIA MENDES ARAÚJO[1,3], ISIS DIDIER LINS[1,3], MÁRCIO DAS CHAGAS MOURA[1,3], AND ENRIQUE LÓPEZ DROGUETT[4,5]

[1]Center for Risk Analysis, Reliability Engineering and Environmental Modeling (CEERMA), Universidade Federal de Pernambuco (UFPE), Recife 50740-550, Brazil
[2]Technology Center, Universidade Federal de Pernambuco (UFPE), Caruaru 55014-900, Brazil
[3]Department of Production Engineering, Universidade Federal de Pernambuco (UFPE), Recife 50740-550, Brazil
[4]Department of Civil and Environmental Engineering, University of California at Los Angeles, Los Angeles, CA 90095, USA
[5]The B. John Garrick Institute for the Risk Sciences, University of California at Los Angeles, Los Angeles, CA 90095, USA

Corresponding author: Isis Didier Lins (isis.lins@ufpe.br)

This work was supported in part by the Human Resources Program (PRH 38.1) through the Agência Nacional de Petróleo, Gás Natural e Biocombustíveis (ANP) and the Brazilian Funding Authority for Studies and Projects (FINEP) under Grant 044819; in part by the Pró-Reitoria de Pós-Graduação (PROPG) of Universidade Federal de Pernambuco under Grant 091849/2022-40; in part by the Foundation of Support for Science and Technology of Pernambuco (FACEPE) under Grant APQ-1101-3.08/21; in part by the Conselho Nacional de Desenvolvimento Científico Tenológico (CNPq) under Grant 3056/2018-1, Grant 309617/2019-7, and Grant 409701/2022-0; and in part by the Coordenação de Aperfeiçoamento de Pessoal de Nível Superior (CAPES) under Finance Code 001.

ABSTRACT Prognostics and Health Management (PHM) concerns predicting machines' behavior to support maintenance decisions through failure modes diagnosis and prognosis. Diagnosis is broadly applied in the context of rotating machines' state classification using several traditional Machine Learning (ML) and Deep Learning (DL) methods. Recently, Quantum Computing (QC), a new and expanding research field, has contributed to different purposes and contexts, such as optimization, artificial intelligence, simulation, cybersecurity, pharmaceutics, and the energy sector. Despite the current limitations in terms of hardware, QC has been studied as an alternative for improving models' speed and computational efficiency. Specifically, this paper proposes a Quantum Machine Learning (QML) approach to diagnose rolling bearings, which are essential components in rotating machinery, based on vibration signals. We apply hybrid models involving the encoding and construction of parameterized quantum circuits (PQC) connected to a classical neural network, the Multi-Layer Perceptron (MLP). We consider combinations of the Variational Quantum Eigensolver (VQE) framework with rotation gates and different entanglement (two-qubits) gates (CNOT, CZ and iSWAP). For each PQC configuration, we assess the impact of the number of layers (1, 5 and 10). We use two databases of different complexity levels not previously explored with QML, namely CWRU and JNU, with 10 and 12 failure modes, respectivel. For CWRU, all QML models presented higher accuracy than the classical MLP. For JNU, all QML models were superior to classical MLP as well. These results suggest that, despite the current limitations of quantum environments, QML models are promising tools to be further investigated in PHM.

INDEX TERMS Quantum machine learning, prognostic and health management, fault diagnosis, vibration signal.

I. INTRODUCTION

Traditionally, policies based on corrective or preventive approaches have been used for reliability and maintenance management. Corrective maintenance deals with unscheduled repairs, which may be time-consuming and expensive, while preventive maintenance does not consider variables that may change over time, such as environmental factors. Alternatively, condition-based maintenance (CBM) [1] is related to predictive maintenance, in which monitoring and

The associate editor coordinating the review of this manuscript and approving it for publication was Yu Zhang.

This work is licensed under a Creative Commons Attribution-NonCommercial-NoDerivatives 4.0 License.
For more information, see https://creativecommons.org/licenses/by-nc-nd/4.0/

analysis of equipment conditions are constantly performed, and decisions are taken when there is a tendency to fail [2]. For example, the Prognostic and Health Management (PHM), applied in the context of maintenance of in-use equipment, aims to avoid system failures and shutdowns [3], [4], [5]. The PHM approach uses a set of raw data obtained on the monitored device and it is within CBM. These data are actual health indicators, and extrapolating them over time enables the definition of decision support for maintenance or the prevention of a severe collapse. We can analyze the models of deterioration progression and forecast the system's status and future operation by utilizing the data.

Rotating machines are essential engineering systems of contemporary and are used in different contexts, such as in the Oil & Gas [6], Aerospacial [7], and Automotive [8] industries. The performance and operational efficiency of rotating machines are significantly impacted by bearings, which account for about 40% of electrical motor failure incidents [9]. Vibrational analysis has become the industry standard for assessing the condition of roller bearings and other rotating machinery. Equipment and components can be better shielded from breaking if bearing issues can be recognized quickly and precisely [10], [11].

Traditional intelligent diagnosis methods include feature extraction using signal processing methods and fault classification by adopting machine learning (ML), and deep learning (DL) approaches [7], [11], [12], [13], [14], [15]. Those methods enable computers to solve problems without explicitly programming a specific problem-oriented algorithm and instead learn from data [8], [16], [17].

For example, Liu et al. [18] used Variational Autoencoder to diagnose failure modes of rotating machinery components. For the same type of equipment, Zhao et al. [11] present a benchmark study with different DL models applied to different databases available in the literature. Among the techniques, multi-layer perceptron (MLP), autoencoder (AE), convolutional neural networks (CNN), recurrent neural networks (RNN), and deep belief networks (DBN) are used.

Recently, important research interest has emerged in the tremendous potential of parallelism offered by Quantum Computing (QC) and related quantum technologies [19]. Quantum algorithms aim to find ways to speed up the solution of computational problems by using a quantum computer [20]. A quantum machine characterizes and computes the quantum characteristic of an atom in a molecule, which is computationally exceedingly challenging even for a supercomputer to handle. This significantly impacts drug research, healthcare, and big data processing [21].

Machine learning and QC are both likely to play a role in how society deals with information in the future, so it is logical to wonder how they could be merged [21], [22], mainly because QC's prospects are increasing faster in hardware performance. For example, it is possible to evaluate several states simultaneously because quantum computations are based on the idea that subatomic particles can exist simultaneously in several states. It may lead to significant speedups [23], conferring, then, a possibility to improve the classic ML [24], since for many scenarios, as the amount of data grows, aligned with the complexity of the information, the training process becomes slower [11]. In this context, ML models with quantum properties have been recently proposed for classification goals [24], [25], [26], [27]. It is one of the many applications that could profit from quantum devices [28]. ML applications incorporating quantum techniques are known as Quantum Machine Learning (QML). QML models are based on QC techniques to develop new algorithms and improve existing ones [25], [26]. Indeed, QC and ML are the two key areas in engineering science as technology is developing quickly [26], [29].

In this paper, we explore the applicability of QML models to diagnose failure modes of different components. Although the subject is promising and has increased its recognition, the research is still limited, among other factors, because of the size of the problems, given the amount of quantum bits (qubits) available in simulators and computers [30]. Note that a qubit is the smallest unit of information in a quantum computer and can be either 0 or 1 or a superposition of these two.

Therefore, we focus on proof of concepts and comparison of the QML with classical techniques evaluated on rotating machine components subjected to vibration as a stressor, common in different industries [6], [31]. To the best of our understanding, this is the first work to present the application of a QML model in the context of PHM classifying more than three health states. Moreover, besides rotation gates, we apply entanglement gates (CNOT, CZ, and *i*SWAP) and more layers in the Parameterized Quantum Circuit (PQC) to observe the effect of such model variations. In addition, our study will be applied to two complex databases available in the literature that have not yet been explored in the context of QML. Those are bearing datasets: (1) Case Western Reserve University (CWRU) [32] and (2) Jiangnan University (JNU) [33]. The results obtained from the application of these models aim to indicate the QML's usability and importance in supporting decision-making related to maintenance.

The remainder of this article is organized as follows. In Section II, there is an overview of the related works. In Section III, we focus on the main concepts of QC. Section IV presents the structured methodology for this work, including the framework used for the QML models, as well as the description of the databases and features used. Section V shows the applications and results. Finally, Section V-C summarizes the main findings of the work and provides some concluding remarks.

II. RELATED WORKS

QC is frequently referred to as an interdisciplinary research frontier involving disciplines as diverse as computer science, physics, chemistry, and engineering. The excitement relies on the hypothesis that quantum information will eventually result in a new wave of technological advancements in information, computation, and communication [34].

QML is a new field of study that emerged by exploiting quantum systems to process classical data using ML techniques. Information processing could be accelerated far beyond current classical speeds [23].

Despite novelty in the context of Reliability Engineering, QML has a growing interest in the academy, with expanding application in recent years. Fig. 1, extracted from Web of Science (WoS), provides the number of articles using ''Quantum Machine Learning'' as a keyword. The first publication appeared in 2014 and, since then, this number has been increasing significantly. The year 2022 has the peak of publications, with 130 in total, despite the search was conducted until October 2022.

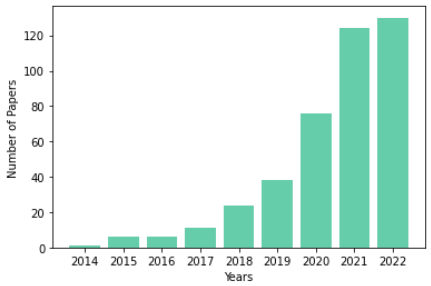

FIGURE 1. "Quantum machine learning" publications in web of science.

The research community has shown interest in two QML strategies. In the first, PQC, a quantum circuit made up of parametric gates is considered a trainable model, with the parameters being updated to minimize a specified objective function. PQC enables researchers to draw obvious similarities and parallels with classic neural networks The second strategy is related to quantum kernel techniques, which can be employed for prediction and tasks like clustering or dimensionality reduction, [26], [27].

Although these combined algorithms have theoretically demonstrated performance gains, their scalability is still in question because current Quantum Processing Units (QPUs) are unable to dependably execute the operations necessary to evaluate these methods on actual data. This is because qubits are still scarce resources and the connectivity between them is constrained [21], [35]. Nevertheless, we can examine the effects of incorporating quantum circuits as building blocks by employing small, parameterized quantum circuits that are easily operated on real hardware or simulated in classical computers. In a sense, this procedure is comparable to what happened with DL models in the wake of ML models' natural progression toward greater scalability around 2010 [25], [26], [36].

In a literature review, when searching by keywords in WoS, the combinations ''Quantum Machine Learning'' and ''PHM'' or ''Fault Detection'' only returned one article. The authors applied quantum kernel methods to wind turbine fault detection [27]. Extending the search to Google Scholar, we found one more article that explores rotating machines [26]. In QML models, the quantum part aims to provide trial states for the algorithm. The PQC, or ansatz circuit, generates these states according to a set of control parameters that are managed by the classical part of the algorithm [37].

PQC has been applied in the PHM context to categorize health states in rotating machinery with performance comparable to conventional ML methods [26]. Nevertheless, in this case, only rotation gates were used. The latter are single qubit parametric gates, whose effect can be externally controlled [27].

Hence, it is necessary to observe the effect of operations such as superposition and entanglement to emphasize the quantum contribution of the model [21], [38]. The ability to be in superposition is one of the qualities that distinguish a qubit from a conventional bit. One way to conceptualize a quantum state in superposition is as a linear combination of other unique quantum states. The core idea is that a search algorithm can tunnel through energetic barriers to escape local minima because quantum superposition and tunneling enable direct transitions between states even when there is a high energy barrier between them [39].

Entanglement is the phenomenon where two particles can be connected independent of the distance [21]. The hypothesis is that the time and computing power needed will be reduced since one qubit can provide information about the other unit to which it is related [23]. In this sense, there are two-qubit gates, such as CNOT and CZ [27].

Faced with the different ways of schematizing PQCs, there are algorithms that combine different types of gates, such as the Variational Quantum Eigensolver (VQE), that can combine the single-qubit and two-qubit, as well as the parameterized and non-parameterized gates [37], [40]. For example, Rasmussen and Zinner [37] used VQE with both single (rotation gates) and two-qubit (CNOT, CZ, and *i*SWAP) gates with angles to be parameterized during training. Meanwhile, Sim et al. [41] performed several combinations with different rotation gates, in x, y, and z, and entanglement gates (CNOT and CZ), forming 19 different circuit types for testing. Schuld and Petruccione [42] also add other circuit schematization possibilities, such as those based on the Quantum Approximate Optimization Algorithm (QAOA) architecture.

III. QUANTUM COMPUTING

If the ability to simulate classical computers were the only feature of quantum computers, there would be little point in going to all the trouble of exploiting quantum effects. The advantage of QC is that much more powerful functions may be computed using qubits and quantum gates [43].

The performance mechanisms in resolving important industrial problems are highlighted by the distinctions between classical computing and QC. The QC mechanics use fundamental quantum properties like superposition, entanglement, and the measurement paradox to find the best answers to challenging issues [43], [44].

Eq. (1) provides the qubit state representation [43], [45], [46]:

$$| \psi\rangle = \alpha \mid 0\rangle + \beta|1\rangle \tag{1}$$

where α and β are complex numbers that represent amplitudes, and they satisfy the relation $|\alpha|^2 + |\beta|^2 = 1$; thus, $|\alpha|^2$ and $|\beta|^2$ are the probabilities of a qubit collapsing to states "0" or "1," respectively, after a measurement. Eq. (1) can be rewritten as Eq. (2), in which the parameters θ, ϕ, and γ are real numbers [25], [39], [43]:

$$| \psi\rangle = e^{i\gamma}(\cos\frac{\theta}{2}\ |0\rangle + e^{i\phi}\sin\frac{\theta}{2}|\ 1\rangle) \tag{2}$$

The Bloch Sphere (Fig. 2) is a geometric representation of the pure state space of a two-level quantum mechanical system. It is used in quantum mechanics and computation [47]. In Fig. 2, the angles θ and ϕ correspond to spherical coordinates that represent a point describing a single qubit state [43]. The $| \psi\rangle$ can be defined as a Hilbert Space vector coming from the origin to the sphere's surface. This vector has a $\mathbb{R}^3$ dimension with the following configuration: [sin(θ)cos(ϕ), sin(θ)sin(ϕ), cos(ϕ)] [42].

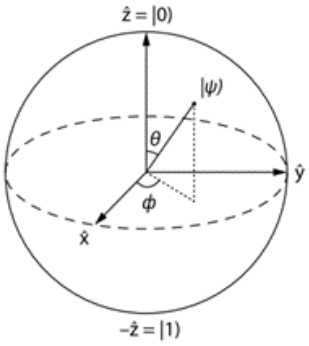

FIGURE 2. Bloch sphere which represents the qubit [43].

Also, the Bloch sphere provides a visual representation of quantum states operations. Rotations on the sphere represent unitary transformations, while projections onto one of the poles depict measurements. The Bloch sphere's utility lies in its ability to show the impact of quantum gates, which form the foundation of quantum circuits. This makes it a valuable tool for creating and examining quantum algorithms and error correction techniques [35], [47]. Finally, The Bloch sphere viually represents entangled states between two quantum systems. When two systems are entangled, their combined state cannot be described by a single point on the sphere but by a region of it [41].

In Fig. 3, one can see a representation of a quantum circuit. The circuit is a QC paradigm comparable to classical circuits, in which a computation is made up of a series of qubit initializations, quantum gates, and measurements to translate the quantum information to classical values. The circuit is read from left to right. For example, following the horizontal lines in Fig. 3, $|0\rangle$ represent the input qubits in state "0." Next are logic gates, such as single-qubit blocks Hadamard (H), X and Z gates, and two-qubit gates as CNOT. In summary, the measurement operation at the end of the line translates the quantum result into a classical one [48].

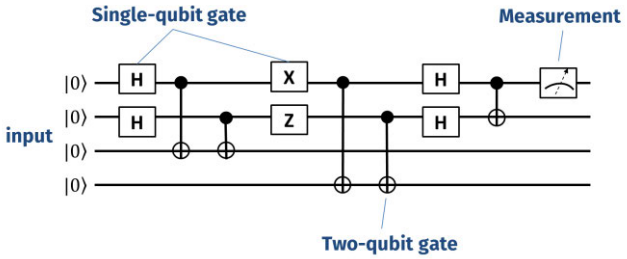

FIGURE 3. A quantum circuit example [48].

A qubit is unusable except if one is able to use it to conduct a quantum computation. These quantum operations are done according to a series of foundational operations called quantum logic gates. They are the building blocks behind all quantum algorithms [20], [36]. The following sections present some of these gates, namely, superposition, controlled, and rotation gates.

A. THE HADAMARD GATE

A new quantum state is created by this superposition [34], [39]. A qubit can be forced into a superposition state using the Hadamard gate. When applied over $| \psi\rangle = | 0\rangle$, its output is a qubit with an equal chance of going from a $|0\rangle$ or $|1\rangle$ state following a measurement [26], [49].

$$H = \frac{1}{\sqrt{2}}\begin{bmatrix} 1 & 1 \\ 1 & -1 \end{bmatrix} \tag{3}$$

B. CONTROLLED GATES

Entanglement is another important quantum mechanics property that is leveraged in QC for constructing dependencies between qubits [27]. Among the entanglement gates, we can cite CNOT, CZ, and *i*SWAP as examples [37].

Two inputs and two outputs make up the CNOT gate. If both qubits are in their absolute basal states, which are either $|0\rangle$ or $|1\rangle$, then the first qubit serves as the control qubit and the second acts as the controlled qubit. If the first qubit is $|0\rangle$, then the CNOT gate does not affect the system; if it is $|1\rangle$, the second qubit is inverted to the opposite state. That is if the second qubit was $|0\rangle$ it becomes $|1\rangle$; if it was $|1\rangle$, it becomes $|0\rangle$ [26], [27].

Target and controlled gates make up the CZ gate. If the controlled gate is 1, a Z gate is applied to the qubit on the target gate. A symmetric gate, the *i*SWAP switches two-qubit states and define the amplitudes of $| 01\rangle$ and $| 10\rangle$ by i [37], [48]. Equations (4)-III-C present the matrices corresponding to these gates.

$$CNOT = \begin{bmatrix} 1 & 0 & 0 & 0 \\ 0 & 1 & 0 & 0 \\ 0 & 0 & 0 & 1 \\ 0 & 0 & 1 & 0 \end{bmatrix} \tag{4}$$

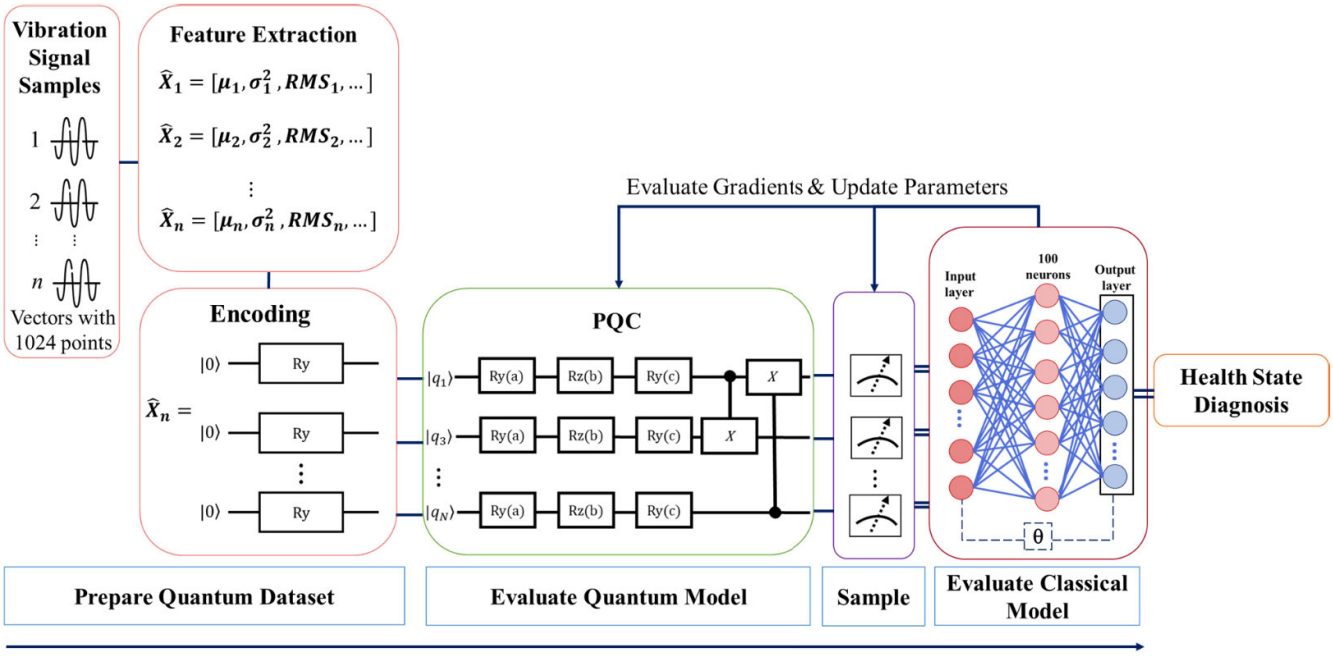

FIGURE 4. Hybrid quantum machine learning scheme to perform health state diagnosis.

$$CZ = \begin{bmatrix} 1 & 0 & 0 & 0 \\ 0 & 1 & 0 & 0 \\ 0 & 0 & 1 & 0 \\ 0 & 0 & 0 & -1 \end{bmatrix} \quad (5)$$

$$iSWAP = \begin{bmatrix} 1 & 0 & 0 & 0 \\ 0 & 0 & i & 0 \\ 0 & i & 0 & 0 \\ 0 & 0 & 0 & 1 \end{bmatrix} \quad (6)$$

C. ROTATION GATES

Since the Hadamard and C-NOT gates work directly on qubits without requiring the definition of external parameters, they can be categorized as non-parametric gates. Rotation gates, on the other hand, can have their impact on a qubit fine-tuned externally, making them single qubit parametric gates [26], [27], [46].

The effect of the rotational gate operation can be simply understood due to the Bloch Sphere depiction. Each operation rotates the qubit by a specific number of radians determined by the external parameter. This rotation is around the considered axis. Eq. (7)-(9) provide the matrices for these gates [26], [27], [46].

$$R_x(\xi) = \begin{bmatrix} cos\frac{\xi}{2} & -isin\frac{\xi}{2} \\ -isin\frac{\xi}{2} & cos\frac{\xi}{2} \end{bmatrix} \quad (7)$$

$$R_y(\xi) = \begin{bmatrix} cos\frac{\xi}{2} & -sin\frac{\xi}{2} \\ sin\frac{\xi}{2} & cos\frac{\xi}{2} \end{bmatrix} \quad (8)$$

$$R_z(\xi) = \begin{bmatrix} e^{-i\frac{\xi}{2}} & 0 \\ 0 & e^{i\frac{\xi}{2}} \end{bmatrix} \quad (9)$$

IV. METHODOLOGY

A. QML FRAMEWORK

The step-by-step framework application of QML models is presented in Fig. 4. This is a framework based on different studies that use the PQC logic in QML models [21], [22], [26]. However, in our case, several modifications were implemented regarding the neural network used, PQC settings, and health status diagnosis. In fact, the applications we present in Section V involve a more complex problem for which more than ten different health states are possible for the machinery diagnosis. Moreover, while in other studies only rotation gates were used [26], [50], we aggregate two-qubit gates – CNOT, CZ, and *i*SWAP – to observe the impact of quantum effects arising from entanglement on the performance of the QML models. In terms of application, we used the Python® programming language along with the TensorFlow Quantum (TFQ) library [22]. Each stage of Fig. 4 is described below:

- Prepare Quantum Dataset: consists of pre-processing the classical data. For example, normalization, dimensionality reductions, and feature extraction can be performed. $\widehat{X}_1, \widehat{X}_2, \ldots, \widehat{X}_n$ are vectors or multidimensional matrices, with a certain number of features monitored. Then, the data is encoded into qubits. A circuit is generated which takes as input N qubits defined in a $|0\rangle$ state and an N-dimensional real-valued vector, whose values lie in a range (e.g., [0, 1]). Encoding schemas are a hot active debated topic that straddles the line between quantum hardware and

software [23]. Various methods could be utilized, such as amplitude encoding and angle encoding. We employed angle encoding. The data processing capabilities of quantum neural networks can directly benefit from this encoding method. This encoding's key advantage is that it is extremely effective in terms of operations because, regardless of the many data values to be encoded, just a fixed number of parallel processes are required [22]. Eq. (10) summarizes the angle encoding method, in which $\otimes$ represents the tensor product between the vector spaces S:

$$\vec{x} \rightarrow |\psi\rangle = S(x_0) \otimes S(x_1) \otimes \ldots \otimes S(x_{N-1}) \tag{10}$$

In Eq. (10), S represents the following operation performed for each element of the classical vector:

$$S(x_i) = \cos\left(\frac{\pi}{2}x_i\right)|0\rangle + \sin\left(\frac{\pi}{2}x_i\right)|1\rangle \tag{11}$$

• Evaluate quantum model: after encoding the data, PQC is created. PQC consists of one or several logic gates where the parameters of the gates (e.g., an angle θ of a rotation Y) are free parameters to be adjusted/optimized depending on the error propagated from outside to inside the circuit. In this study, we tested different PQC schemes. The first one consists only of rotation gates in y, x, and z, for each qubit (q_i), as shown in Fig. 5. Note that a, b and c are the angles of each gate to be parameterized.

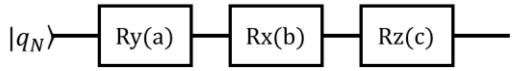

FIGURE 5. PQC defined by y, x and z rotation gates.

In addition, we considered the circuit configuration used in the VQE quantum algorithm based on the study by Rasmussen and Zinner [37]. First, an Euler rotation is performed on each qubit, followed by a nearest-neighbor coupling using the given entangling gate. Here, we apply the two-qubit gates C-NOT, CZ, and iSWAP as shown in Fig. 6. PQCs were built with different numbers of layers, namely, 1, 5, and 10.

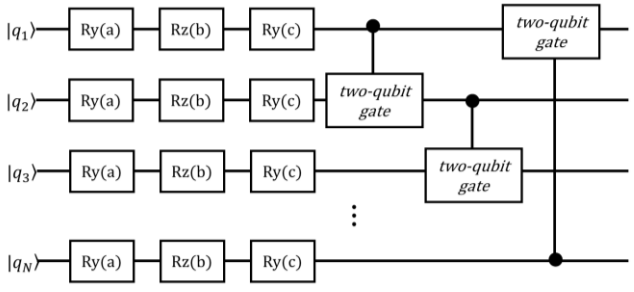

FIGURE 6. PQC defined VQE with generic two-qubit gates visualization that in this study can be CNOT, CZ, or iSWAP.

• Sample or Average: measurements are performed, returning the processed quantum data to classical data. For this work, a measurement operation was defined through the Pauli Z-gate (Eq. (12)) in each of the qubits. Pauli measurements are a generalization of computational basis measurements that cover measurements in other bases and of equality between several qubits. A measurement in the Pauli Z basis projects the state onto one of the eigenstates $|0\rangle$ or $|1\rangle$ of this matrix [48]:

$$Z = \begin{bmatrix} 1 & 0 \\ 0 & -1 \end{bmatrix} \tag{12}$$

• Evaluate classical model: the classical model is a neural network. Features extracted from the database and encoded are inserted into the neural network. In this process, back-propagation is flowed through the weights of the neural network and into the PQC.

B. ROTATING MACHINERY DATABASES

With their widespread use and research in industrial applications, rolling bearings are a crucial and vital part of rotating equipment [18]. Information is acquired using a variety of techniques, which can be roughly categorized based on the measurements made: temperature, wear debris analysis, vibration, and acoustic measures [6]. Due to their easy-to-measure signals and convincing analysis, vibration measurements are among those that are frequently utilized in the condition monitoring and diagnosis of rotating machinery [7], [51], [52].

In this context, public datasets are available for intelligent diagnosis. Indeed, assembling several types of representative datasets is crucial for complete performance comparisons [11]. In this study, the performance of the models is analyzed using two datasets: CWRU and JNU.

1) CWRU DATASET

The Bearing Data Center dataset from Case Western Reserve University (CWRU) [32] is well-known in the PHM literature and is used here to assess the proposed methodology. The set includes signals from mechanical vibration series obtained from an induction electric motor with engine load starting from 0 to 3 HP. Data were obtained from two accelerometers mounted on top of the motor and connected by magnetic bases, one of which was collected at the drive end (DE), and the other was collected nearby the bearing fan end (FE). The collections of the two accelerometers are precisely coordinated.

These faults, which can occur in the rearing rolling element (RE), the inner raceway (IR), and the outer raceway (OR), are intentionally introduced by an electro-discharge machine This operation is applied at different motor rotation rates. The faults generated have different diameters [32].

Table 1 shows the different failure modes, diameters and proportion of each class in the data set. The vibration data are collected at a rate of 12k samples per second from accelerometers connected to the equipment at two points: the upper and lower turbine of the device. For our application, we consider the case of 1797 rpm and 0 HP.

TABLE 1. Description of failure modes of the CWRU [11], [32].

Label	Mode Description	Proportion (%)
0	Health State: the normal bearing	18.24
1	Inner ring 1: 0.007 inch	9.04
2	Inner ring 2: 0.014 inch	9.12
3	Inner ring 3: 0.021 inch	9.12
4	Rolling Element 1: 0.007 inch	9.04
5	Rolling Element 2: 0.014 inch	9.04
6	Rolling Element 3: 0.021 inch	9.04
7	Outer ring 1: 0.007 inch	9.12
8	Outer ring 2: 0.014 inch	9.12
9	Outer ring 3: 0.021 inch	9.12

2) JNU DATASET

Jiangnan Universit's (JNU) [11], [33], [53] bearing datasets is also freely available and are made up of three vibration datasets with three different rotating speeds (600, 800, and 1000 rpm), all of which were gathered at 50 kHz. One health condition and three failure modes are displayed in the JNU datasets (IR, OR, and RE). All states were measured at the same locations as the CWRU base. As a result, the total working conditions classes are twelve, as shown in Table 2 with the respective proportions for each state.

TABLE 2. Description of failure modes of the JNU [11].

Label	Mode Description	Proportion (%)
0	Inner ring 1: 600 rpm	5.55
1	Health State 1: 600 rpm	16.68
2	Outer ring 1: 600 rpm	5.55
3	Rolling Element 1: 600 rpm	5.55
4	Inner ring 2: 800 rpm	5.55
5	Health State 2: 800 rpm	16.68
6	Outer ring 2: 800 rpm	5.55
7	Rolling Element 2: 800 rpm	5.55
8	Inner ring 3: 1000 rpm	5.55
9	Health State 3: 800 rpm	16.68
10	Outer ring 3: 1000 rpm	5.55
11	Rolling Element 3: 1000 rpm	5.55

C. FEATURE EXTRACTION

Standard vibration-based metrics like mean, variance, root mean square (RMS), variance, kurtosis, as well as higher-order statistics, are frequently employed for machinery diagnostics. In this study, we use eight different features, which are described below.

- Variance and Mean: the statistical dispersion of a signal is measured by variance [54]. The impacts in a spalled bearing should increase the signal's variability. The variance for a time series s_i with length L is:

$$\sigma^2 = \frac{1}{L}\sum_{i=1}^{L}(s_i - \bar{s})^2 \tag{13}$$

where the population mean, i.e., the average of the signal values [55], [56], is:

$$\bar{s} = \frac{1}{L}\sum_{i=1}^{L} s_i \tag{14}$$

- RMS: it is the square root of the mean square, i.e., the arithmetic mean of the squares of the data. Also, it represents the residual signal energy [57], [58]:

$$RMS = \sqrt{\frac{1}{L}\sum_{i=1}^{L} s_i^2} \tag{15}$$

- Skewness (SKW): it describes a distortion or asymmetry in a set of data that departs from the normal distribution. The curve is said to be skewed if it is displaced to the left or right [59]. It can be calculated as follows [56]:

$$SKW = \frac{\frac{1}{L}\sum_{i=1}^{L}|s_i - \bar{s}|^3}{\left(\sqrt{\frac{1}{L}\sum_{i=1}^{L}|s_i - \bar{s}|^2}\right)^3} \tag{16}$$

- Kurtosis: is frequently used as an indicator for quantifying vibration signal impulses [60]. It represents how far the distribution's tails diverge from the normal distribution's tails [61], [62]. Kurtosis is defined as follows:

$$Kurtosis = \frac{(L-1)\sum_{t-1}^{L}(s(t) - \bar{s})^4}{\left(\sum_{t-1}^{L}(s(s(t) - \bar{s}) - \bar{s})^2\right)^2} \tag{17}$$

- Peak-to-peak (PP): is the difference between a waveform's maximum positive and maximum negative amplitudes [57], and it is calculated according to:

$$PP = s_{max} - s_{min} \tag{18}$$

- Maximum Amplitude: is the maximum displacement or distance moved by a point on a vibrating body or wave measured from its equilibrium position [9]. The notation for this feature is:

$$MaxAmp = s_{max} \tag{19}$$

- Crest Factor: is the ratio of the peak vibration level to the RMS and is frequently used to detect changes in signal patterns caused by impulse vibration sources that are not normally captured by RMS analysis alone. Under normal circumstances, its value ranges between 2 and 6. It is determined as follows:

$$Crest\ Factor = \frac{Peak\ Level}{RMS} \tag{20}$$

V. APPLICATION AND RESULTS

A. CWRU RESULTS

The first data configuration developed for this study encompasses five features: (i) mean, (ii) variance, (iii) maximum

amplitude, (iv) peak-to-peak, and (v) RMS. The second structure used the features from (i)-(v) in addition to: (vi) crest factor, (vii) kurtosis, and (viii) skewness.

The vibration signals were divided into segments of length equal to 1,024 points. The extension of the database resulted in 1,305 samples with the number of columns corresponding to the number of features.

The data was divided into 70% for training, while the remaining 30% were used for testing. Then, angle encoding was performed. The output of this step is a set of objects generated for reading and operation in the quantum circuits. These objects have a bijective relationship with the data points (i.e., each data point has exactly one circuit representation). Fig. 7 shows one example of a database vector with its respective encoding results.

In the end, the traditional neural network recieves as input the classical information obtained from the quantum measurement step. The processing was structured with three layers: the first one consists of the input units that depends of the number of the model features (5 or 8); the second has 100 neurons; and, finally, the output layer has the number of neurons equivalent to the number of classes (10 and 12 to CWRU and JNU, respectively). The SoftMax activation function computes the scores for each class. Thus, the model provides the prediction of the corresponding failure mode.

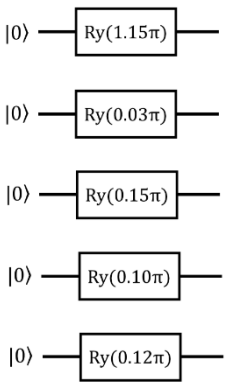

FIGURE 7. Vector with angle encoding.

TABLE 3. Neural network setup.

Neural Network Setup	
Input Layer Neurons:	Nº of qubits (5 or 8)
Hiden Layer Neurons:	100
Ouput Layer Neurons:	Nº of classes (10 or 12)
Activation function:	SoftMax
Loss function:	Cross entropy categorical
Optimizer:	Adam
Learning Rate:	0.01
Epochs:	300
Batch size:	32
Patience (Early Stop):	30

The cross-entropy categorical function is used to measure the models' losses. The default backpropagation operation of TFQ considers the PQC as a black box. It uses the finite difference method to compute the gradient approximation corresponding to the free parameters (rotation gates angles to parameterized: a, b, and c). Adam optimizer was used, with a learning rate of 0.01. We ran the training for 300 epochs, with the patience of 30 epochs for an early stop. The above configuration is summarized in Table 3. For comparison purposes, the same structure was considered to represent the classical model (i.e., MLP).

Table 4 shows the accuracy, precision, recall, and F1-score results obtained when running the classic ML and QML models. Initially, the lowest accuracy presented is for MLP, resulting in 95.40% and 91.95% for five and eight features, respectively. Among the QML models with five features, the best accuracy (98.08%) is presented in three scenarios: only rotation gates with one layer; and VQE with the CZ gate having one and five circuit layers. However, observing the other metrics, the CZ with five layers had a better-weighted precision than the others.

Considering the first type of QML model (Ry, Rx, Rz), the behavior of the four metrics has better performances on circuits with only one layer and worse ones with ten layers. Thus, showing a decreasing pattern as the number of layers increases. The PQC with CNOT has the lowest accuracy of the QML models when applied to ten circuit layers (95.79%). Increasing this number to 1 peaks the performance to 96.55%. As observed, this result does not improve when increasing the number of layers. The PQC with CZ as the two-qubit gate has its worst result with ten layers and the best with 5 when considering mainly the precision. Finally, the iSWAP has similar behavior to CZ, i.e., the worst result for ten layers. However, best with one and intermediate with ten.

Still, in Table 4, we can observe the results for the model with eight features. In this scenario, MLP also has the worst accuracy (91.95%). The best result consists of the configuration of PQC with CZ and five layers (98.47%), which is approximately six percentage points greater than MLP. Results with eight features were better than those with five features in only six of 13 scenarios.

Table 5 shows all the CWRU confusion matrices (CM) and accuracy curves. In the CMs, for the five features QML models with only rotation gates (Fig. 8a), with CNOT (Fig. 8b), and with CZ (Fig. 8c), the three with one layer, the most severe diagnostic problems were in label 2: IR with 0.014 inches. The worst classification for iSWAP (Fig. 8d), with one layer, was in label 5 (RE2).

The graphs of accuracy in Table 5 show the number of epochs for each model to achieve its best result, according to the stopping criterion used (patience of 30 epochs). Fig. 9 summarizes some of these graphics.

For the circuits with only one layer, one observes that the model with only rotations (Fig. 9a) needed 48 epochs to reach its peak accuracy. The other configurations, on the other hand, varied around 80 epochs. In this case, CNOT

TABLE 4. CWRU: ML and QML Accuracy, Precision, Recall and F1-Score results. Performances change on a color scale from shades of green for the best results, to red for the worst.

Category	Quantum gates	# of circuit layers	Accuracy (%)		Precision (%)		Recall (%)		F1-Score (%)	
			5 features	8 features	5 features	8 features	5 features	8 features	5 features	8 features
Classic ML (MLP)	-	-	95.40	91.95	96.06	92.88	95.40	91.95	95.20	91.48
QML	Ry, Rx, Rz	1	98.08	97.32	98.23	97.48	98.08	97.32	98.08	97.24
		5	96.93	95.02	97.38	95.34	96.93	95.02	96.84	94.88
		10	96.17	96.93	96.49	95.34	96.17	96.93	96.08	96.95
	VQE: Ry, Rx, Rz + CNOT	1	96.55	94.25	96.68	94.60	96.55	94.25	96.49	94.21
		5	96.17	95.02	96.68	95.27	96.17	95.02	96.02	95.03
		10	95.79	95.79	96.21	96.04	95.79	95.79	95.73	95.62
	VQE: Ry, Rx, Rz + CZ	1	98.08	96.93	98.21	97.23	98.08	96.93	98.02	96.90
		5	98.08	98.47	98.26	98.65	98.08	98.47	98.08	98.49
		10	96.17	96.55	96.70	96.83	96.17	96.55	96.20	96.47
	VQE: Ry, Rx, Rz + iSWAP	1	96.55	96.93	96.65	96.99	96.55	96.93	96.54	96.89
		5	96.55	95.79	96.61	96.10	96.55	95.79	96.49	95.72
		10	96.17	96.93	96.65	97.30	96.17	96.93	96.13	96.92

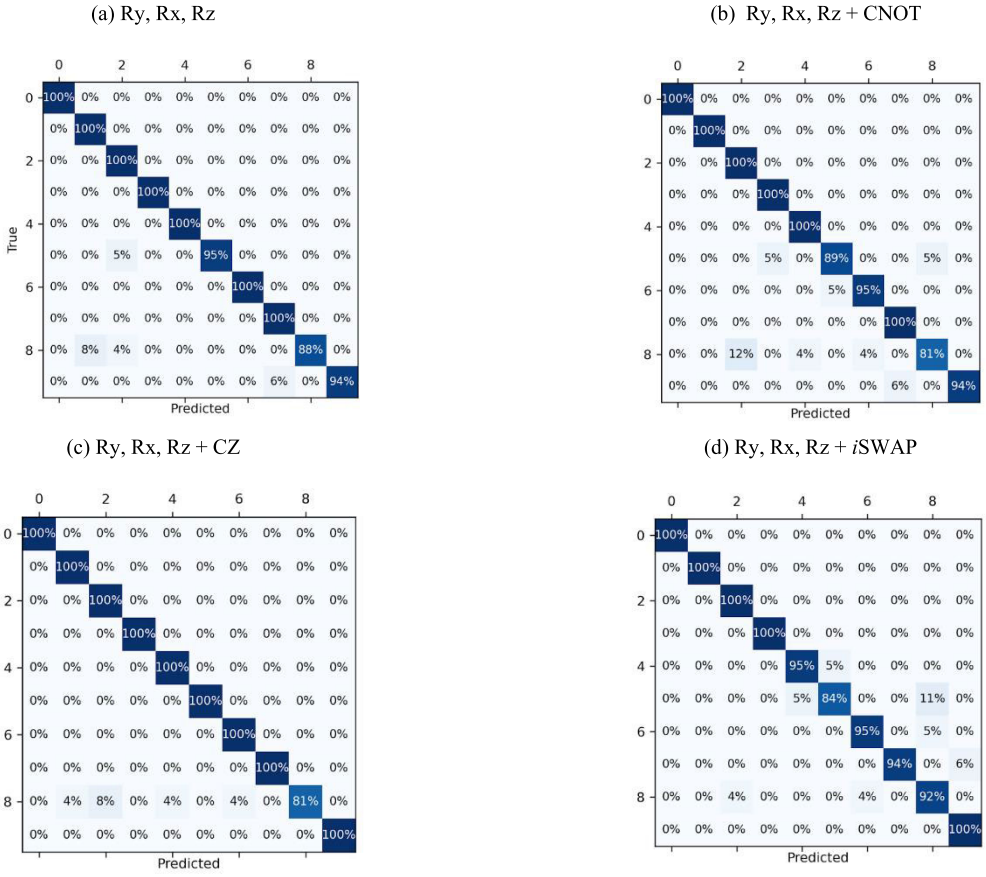

FIGURE 8. CWRU confusion matrices for one layer PQCs for the following configurations: (a) Ry, Rx, Rz; (b) Ry, Rx, Rz + CNOT; (c) Ry, Rx, Rz + CZ; (d) Ry, Rx, Rz + iSWAP.

with 81 (Fig. 9b), CZ with 80 (Fig. 9c), and *i*SWAP with 76 (Fig. 9c). Regarding the circuit repetition, not necessarily more layers need more epochs, as it was not true for the four tested configurations.

TABLE 5. CWRU dataset: confusion matrix and model accuracy graph with five and eight features.

Model	5 features		8 features	
	CM	Accuracy	CM	Accuracy
Ry, Rx, Rz (1 layer)	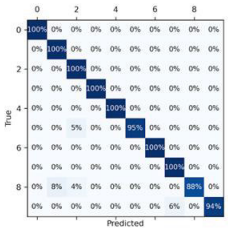	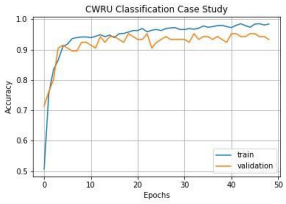	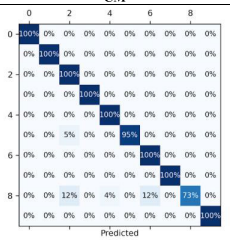	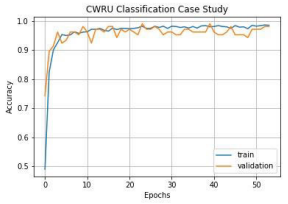
Ry, Rx, Rz (5 layers)	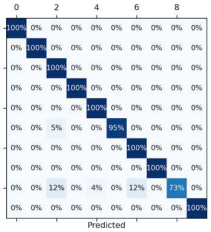	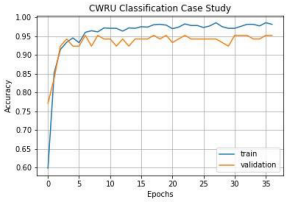	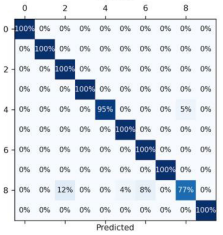	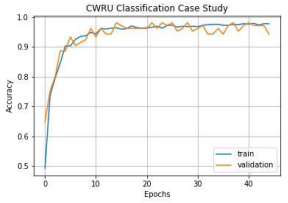
Ry, Rx, Rz (10 layers)	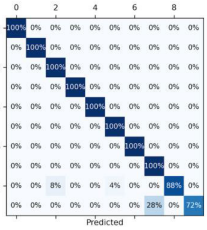	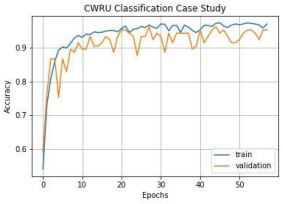	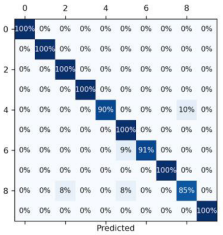	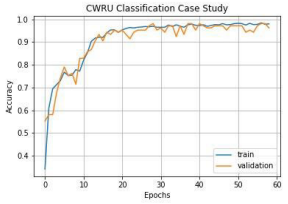
VQE: Ry, Rx, Rz + CNOT (1 layer)	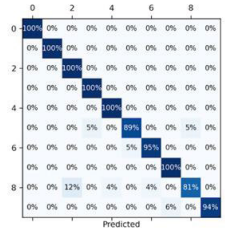	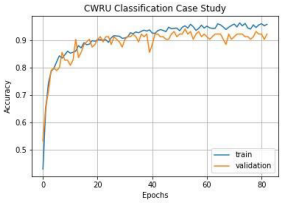	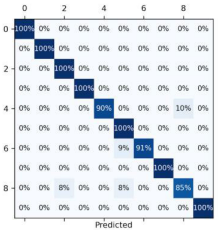	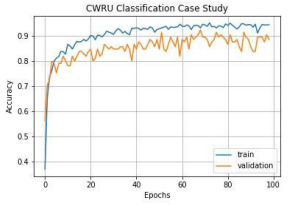
VQE: Ry, Rx, Rz + CNOT (5 layers)	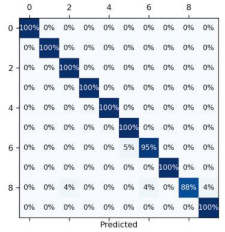	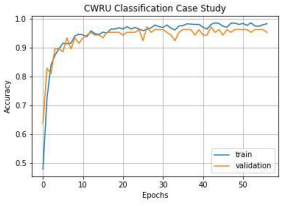	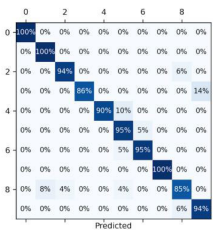	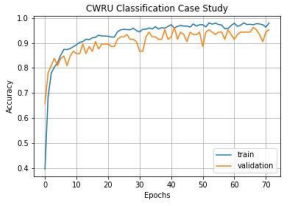
VQE: Ry, Rx, Rz + CNOT (10 layers)	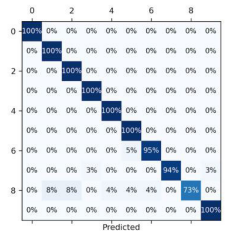	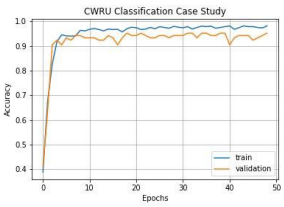		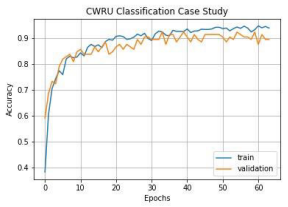
VQE: Ry, Rx, Rz + CZ (1 layer)	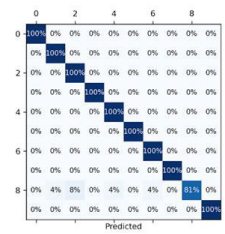	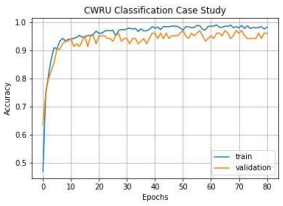	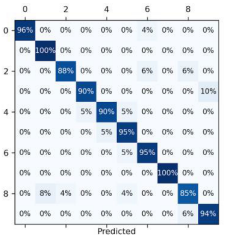	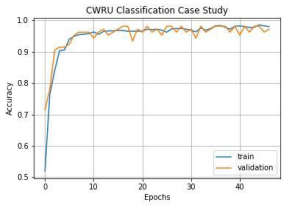

TABLE 5. *(Continued.)* **CWRU dataset: confusion matrix and model accuracy graph with five and eight features.**

VQE: Ry, Rx, Rz + CZ (5 layers)	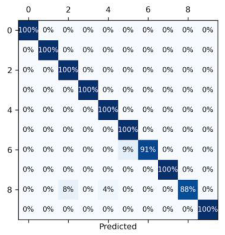	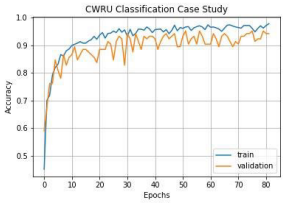	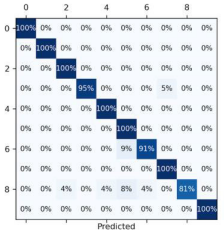	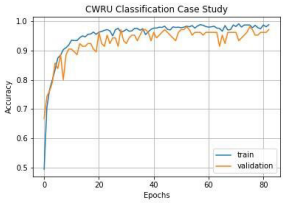
VQE: Ry, Rx, Rz + CZ (10 layers)	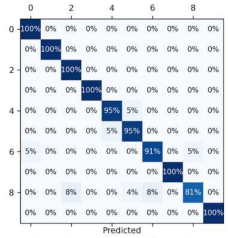	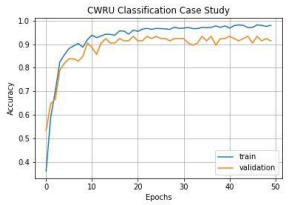	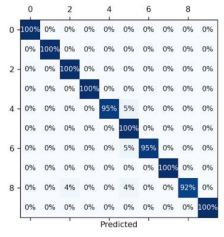	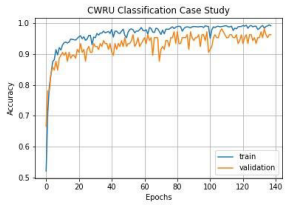
VQE: Ry, Rx, Rz + *i*SWAP (1 layer)	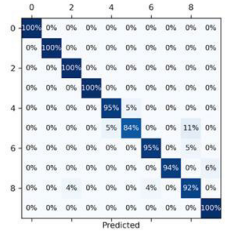	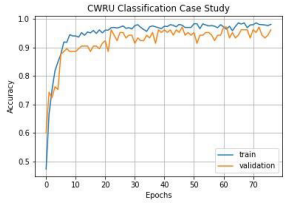	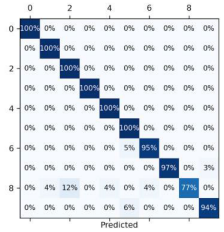	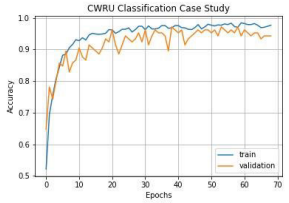
VQE: Ry, Rx, Rz + *i*SWAP (5 layers)	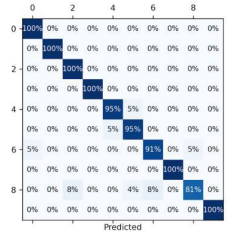	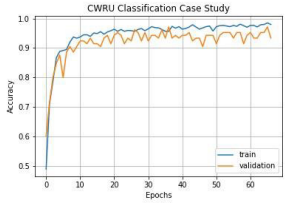	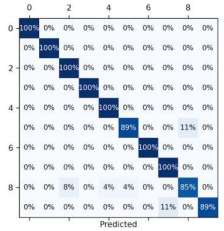	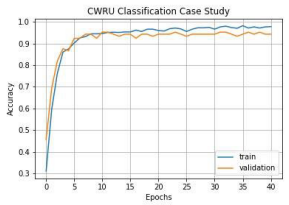
VQE: Ry, Rx, Rz + *i*SWAP (10 layers)	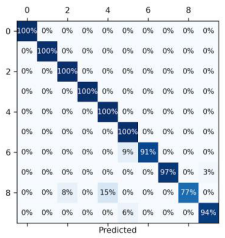	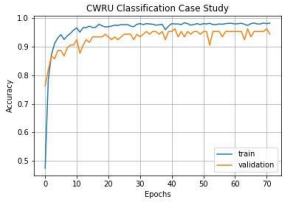	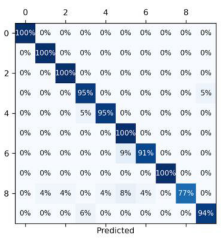	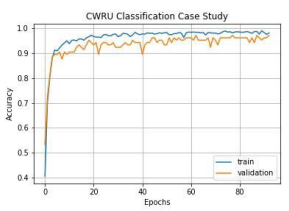

B. JNU DATASET

The settings used for training this database are similar to those of the CWRU. However, this larger database resulted in a sample size of 8,790 rows and 12 health states. Indeed, JNU is a more complex database than CWRU. In a study dealing with seven different databases from the rotating machinery components literature, the authors state that JNU is at 3 out of 4 levels of difficulty, while CWRU is at 1 out of 4 (see Zhao et al. [11]).

Table 6 presents the accuracy, precision, recall, and F1-score results obtained from the Classic MLP and QML models. With five features, the lowest accuracy was obtained for the MLP, resulting in 61.59% of the test data, followed by VQE with CZ with ten layers (62.19%). The best accuracy was in the PQC with the two-qubit gate CZ and one-layer circuit with an accuracy of 70.49%, followed by rotation gates and with iSWAP, both with one layer, that hit 70.31% and 70.27%, respectively. However, when we look at the precision metric, the order of best performance goes first to iSWAP (68.63%), then to VQE with CZ (67.74%), and lastly to just rotation gates (67.70%). For all metrics, the model with the CNOT two-qubit gate is the only one with just intermediate to low values since it does not have any green highlights in Table 6.

With eight features, the worst accuracy was obtained by the same configuration of five features: MLP (62.57%). The second place belongs to the VQE with CNOT with one layer (63.44%). The other metrics follow

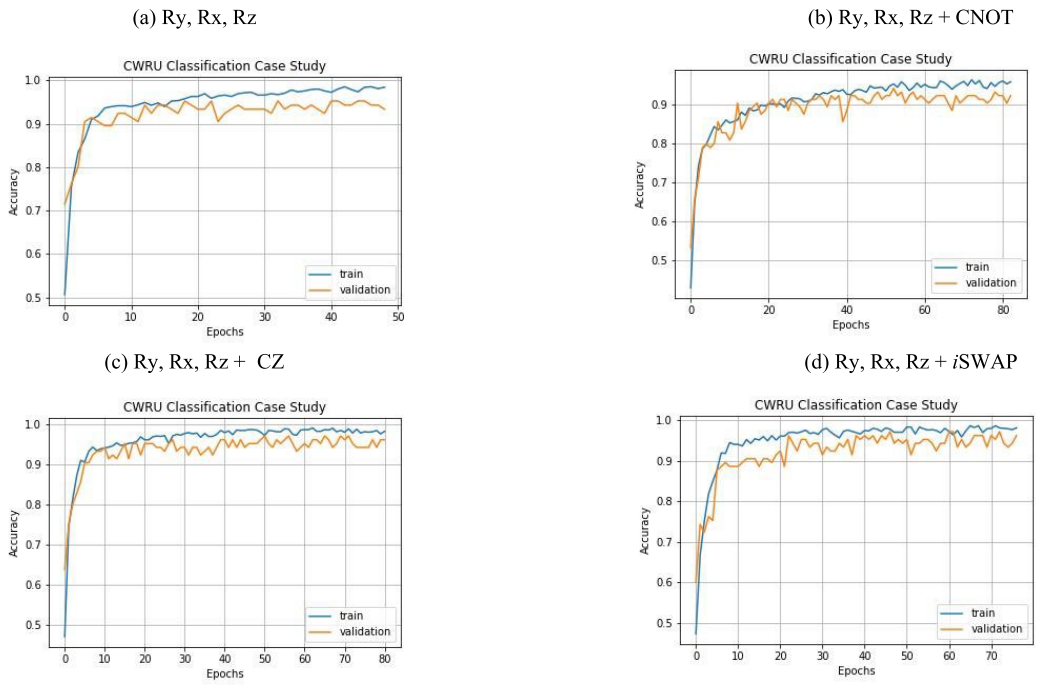

FIGURE 9. CWRU accuracy curves for one layer PQCs for the following configurations: (a) Ry, Rx, Rz; (b) Ry, Rx, Rz + CNOT; (c) Ry, Rx, Rz + CZ; (d) Ry, Rx, Rz + *i*SWAP.

TABLE 6. JNU: ML and QML Accuracy, Precision, Recall and F1-Score results. Performances change on a color scale from shades of green for the best results, to red for the worst.

Category	Quantum gates	# of circuit layers	Accuracy (%)		Precision (%)		Recall (%)		F1-Score (%)	
			5 features	8 features	5 features	8 features	5 features	8 features	5 features	8 features
Classic ML (MLP)	-	-	61.59	62.57	49.91	56.52	61.59	62.57	53.91	56.11
QML	Ry, Rx, Rz	1	70.31	70.04	67.70	67.98	70.31	70.04	68.29	68.08
		5	69.28	69.93	65.47	68.06	69.28	69.93	65.38	67.78
		10	68.49	68.37	65.72	66.10	68.49	68.37	65.91	65.80
	VQE: Ry, Rx, Rz + CNOT	1	63.41	63.44	58.94	58.07	63.41	63.44	57.98	58.37
		5	66.02	65.91	62.13	62.52	66.02	65.91	62.76	61.55
		10	65.19	67.90	61.52	63.93	65.19	67.80	60.68	64.26
	VQE: Ry, Rx, Rz + CZ	1	70.42	68.37	67.74	65.70	70.42	68.37	67.67	65.69
		5	64.88	67.80	59.95	64.41	64.88	67.80	59.88	64.75
		10	62.19	68.41	57.43	65.09	62.19	68.41	58.19	65.58
	VQE: Ry, Rx, Rz + iSWAP	1	70.27	70.19	68.63	67.47	70.27	70.19	67.67	67.98
		5	69.43	67.65	65.89	64.22	69.43	67.65	66.62	63.65
		10	64.92	64.85	59.33	61.89	64.92	64.85	60.42	61.64

the same order. The best accuracy was obtained with the *i*SWAP (one layer) with an accuracy of 70.19%, followed by rotation gates (Ry, Rx, Rz) with one and five layers, corresponding to 70.04% and 69.93%, respectively. However, the accuracy of rotation gates with five layers (68.06%) is better than rotation gates with one layer and *i*SWAP (one layer). The latter two configurations have accuracy in the order previously written, with 67.98% and 67.47%, respectively.

Note that the best precision is approximately 11 percentage points greater than the Classic MLP. In addition, with eight features, increasing metrics performance behavior by adding the layers only happened in the configuration with CNOT.

TABLE 7. JNU dataset: confusion matrix and model accuracy graph with five and eight features.

Model	5 features		8 features	
	CM	Accuracy	CM	Accuracy
Ry, Rx, Rz (1 layer)	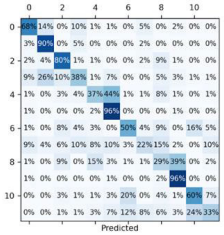	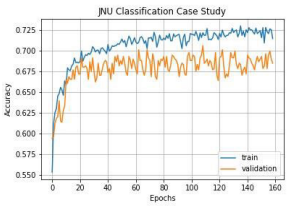	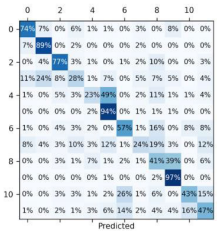	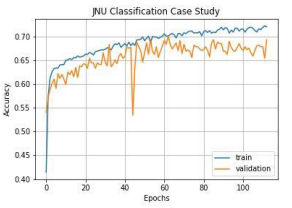
Ry, Rx, Rz (5 layers)	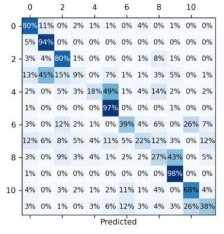	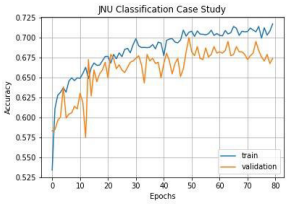	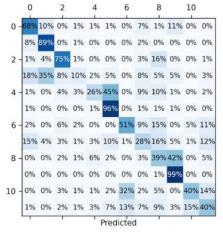	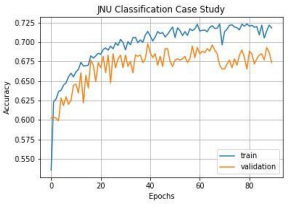
Ry, Rx, Rz (10 layers)	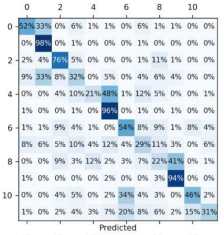	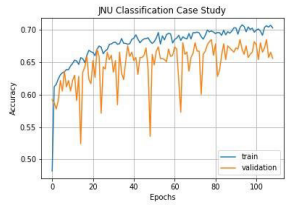	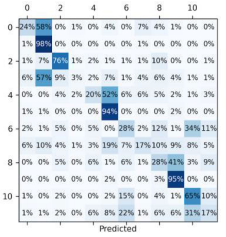	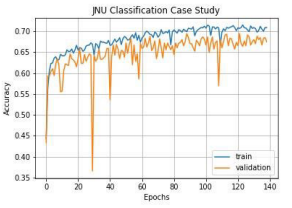
VQE: Ry, Rx, Rz + CNOT (1 layer)	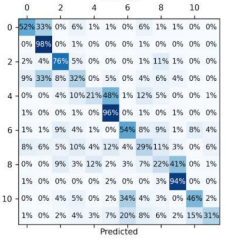	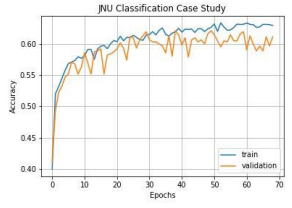	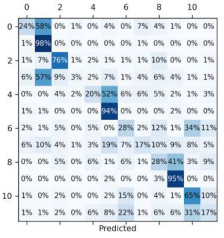	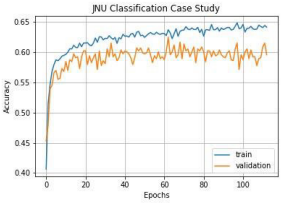
VQE: Ry, Rx, Rz + CNOT (5 layers)	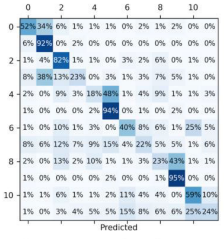	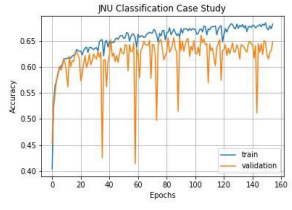	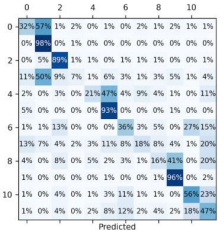	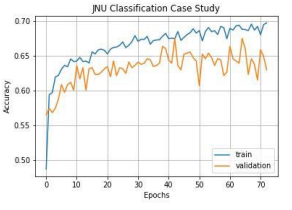
VQE: Ry, Rx, Rz + CNOT (10 layers)	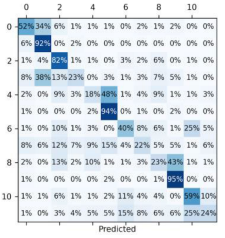	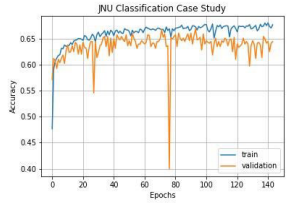	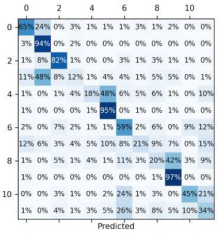	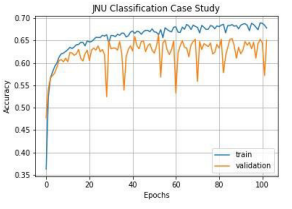
VQE: Ry, Rx, Rz + CZ (1 layer)	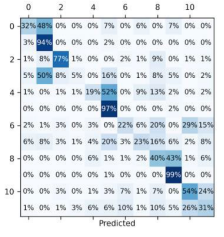	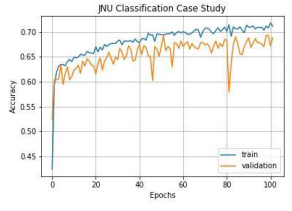	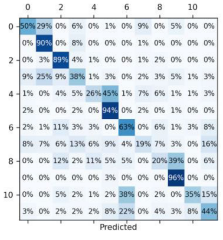	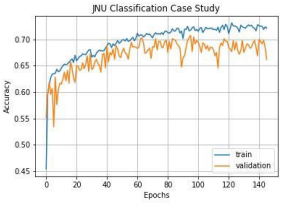

TABLE 7. *(Continued.)* **JNU dataset: confusion matrix and model accuracy graph with five and eight features.**

VQE: Ry, Rx, Rz + CZ (5 layers)	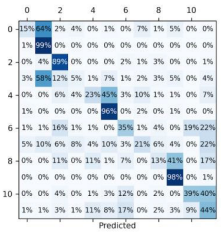	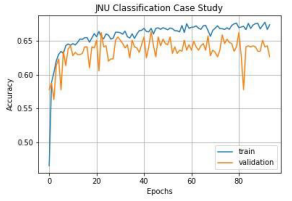	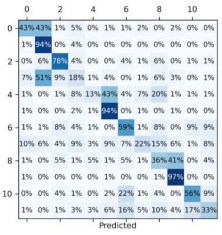	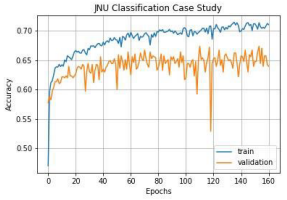
VQE: Ry, Rx, Rz + CZ (10 layers)	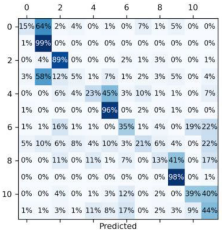	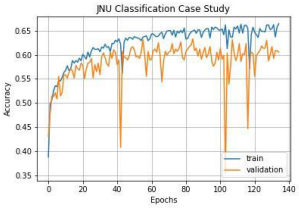	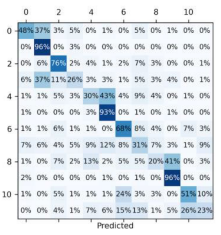	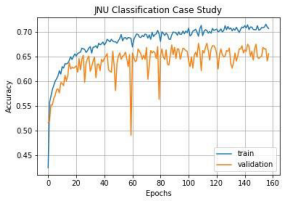
VQE: Ry, Rx, Rz + *i*SWAP (1 layer)	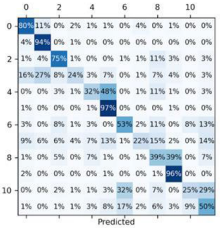	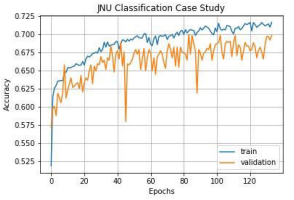	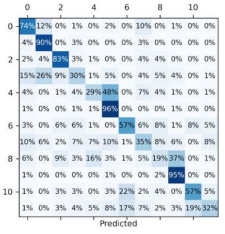	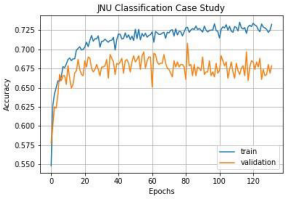
VQE: Ry, Rx, Rz + *i*SWAP (5 layers)	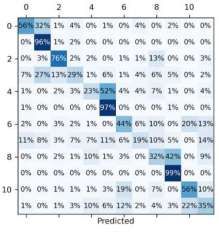	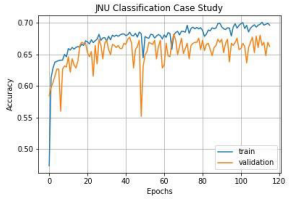	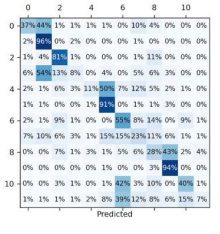	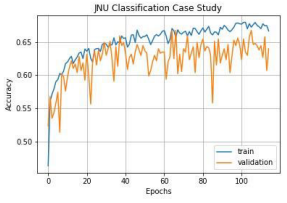
VQE: Ry, Rx, Rz + *i*SWAP (10 layers)	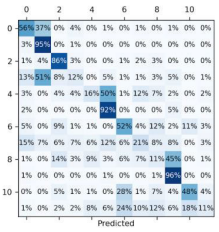	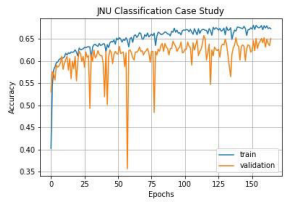	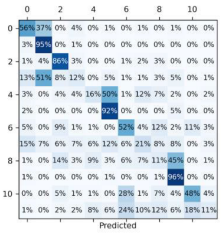	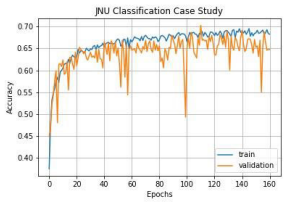

Table 7 presents the JNU confusion matrices and accuracy curves. Concerning the CMs, for the five features QML models with only rotation gates (Fig. 10a) and *i*SWAP (Fig. 10d), both with one layer, the most severe diagnostic problems were in label 7: rolling Element 2 at 800 rpm. For CNOT (Fig. 10b) and CZ (Fig. 10c), it was, respectively, label 4 (inner ring at 800 rpm) and label 3 (rolling element at 600 rpm).

The accuracy graphs in Table 7 display the number of epochs required by each model to produce its best outcome. The more layers in PQCs using *i*SWAP (Fig. 11d), the more epochs are required. However, for only rotation gates (Fig. 11a), VQE with CNOT (Fig. 11b), and VQE with CZ (Fig. 11c), we did not observe such a behavior.

C. DISCUSSION

Here we outline more general considerations of the obtained results presented for each database regarding the trained structures. Note that we base our observations on the content of Tables 4 and 6.

We varied our models in three aspects: (1) the number of features; (2) PQC quantum operations structure; and (3) the number of circuit layers. In (1), since the quantum simulator used cannot process the complete signal, given the limitation of qubits, extracting features is a way to test the QC models. We use these two types of inputs, 5 and 8 features, to infer if a larger amount would yield better metric results.

In the classical model (MLP), different behaviors occurred in the two databases: the results with five features were better

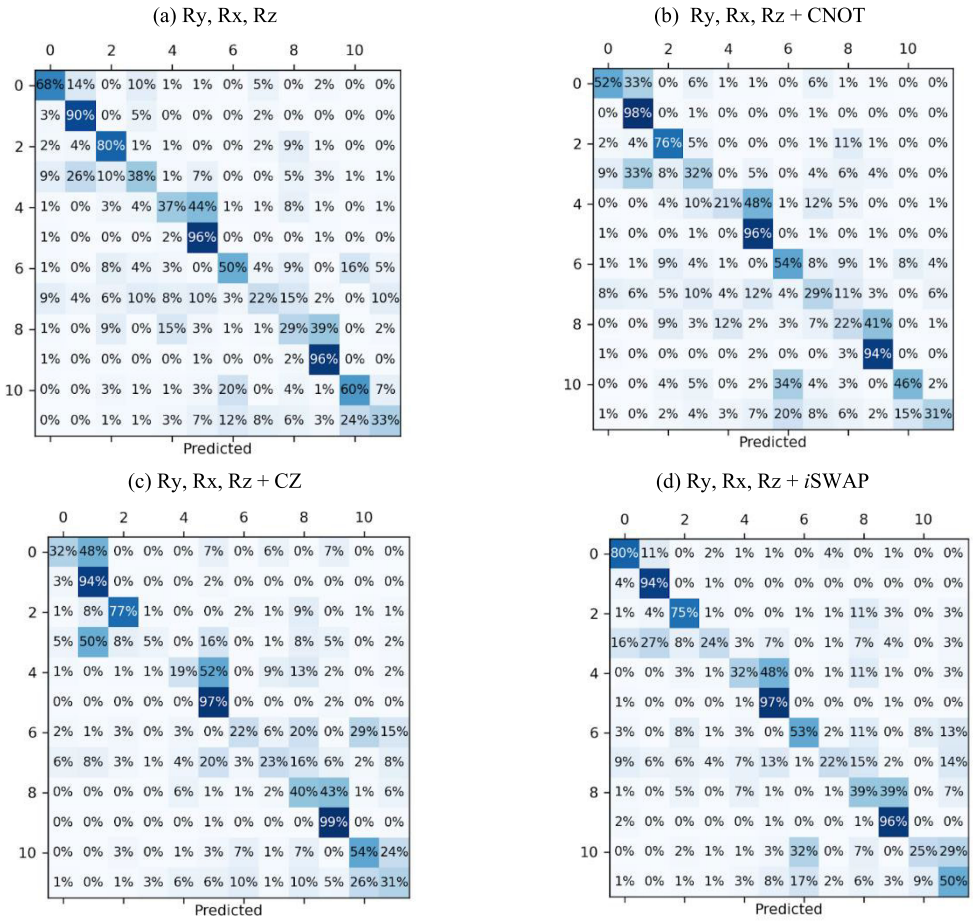

FIGURE 10. JNU confusion matrices for one layer PQCs for the following configurations: (a) Ry, Rx, Rz; (b) Ry, Rx, Rz + CNOT; (c) Ry, Rx, Rz + CZ; (d) Ry, Rx, Rz + iSWAP.

in all metrics for CWRU, while in JNU, it was the opposite. For the quantum models, on the other hand, this varied. In the CWRU, when considering the precision metric, the results with five features were better than the eight features results since they were successful in 58.33% of the cases. For JNU, in turn, results with eight features were the ones that obtained this percentage. But when observing the recall, for example, in CWRU, in six out of 12 scenarios, the results with eight features were better, and in one of them, the results were equal. In JNU, five features came out on top, with seven out of 12 results.

For the analysis of quantum operations, merging points (2) and (3) is interesting. We can clearly identify in Tables 4 that the model with the CZ entanglement gate and five layers has the greenest results in CWRU in all calculated metrics. The frameworks that followed it involved only rotations in a single layer and the CZ itself with one layer.

Zooming in on each of the models, starting with just rotation gates, one sees that with five features, the behavior of the results is decreasing. With eight features, this varies a bit, but generally, the best performances are with only one layer.

The model with CNOT is one of the worst overall; the results mostly vary from yellow to reddish, with no green points. As said before, the entanglement gate gains prominence, especially in the scenario with five layers. And its worst results are in the increase to 10 layers. Finally, iSWAP shows average results with some highlights, mainly with eight features.

In JNU, Table 6, the highlights in green are divided between just rotations, followed by *i*SWAP, CZ, and again, lastly, CNOT. In most cases with just rotations, the behavior when varying the layers is also mostly decreasing, i.e., the best results remain in the first layer as in CWRU. The same is true for CZ and *i*SWAP. In CNOT, however, this changes somewhat, as the negative highlights this time are in the first layer.

Thus, overall, the scenario with the rotation gates did relatively well for the two databases. CZ got the best accuracy values, but at some points, especially for JNU, it had very reddish values. It is seen that CNOT did not manage

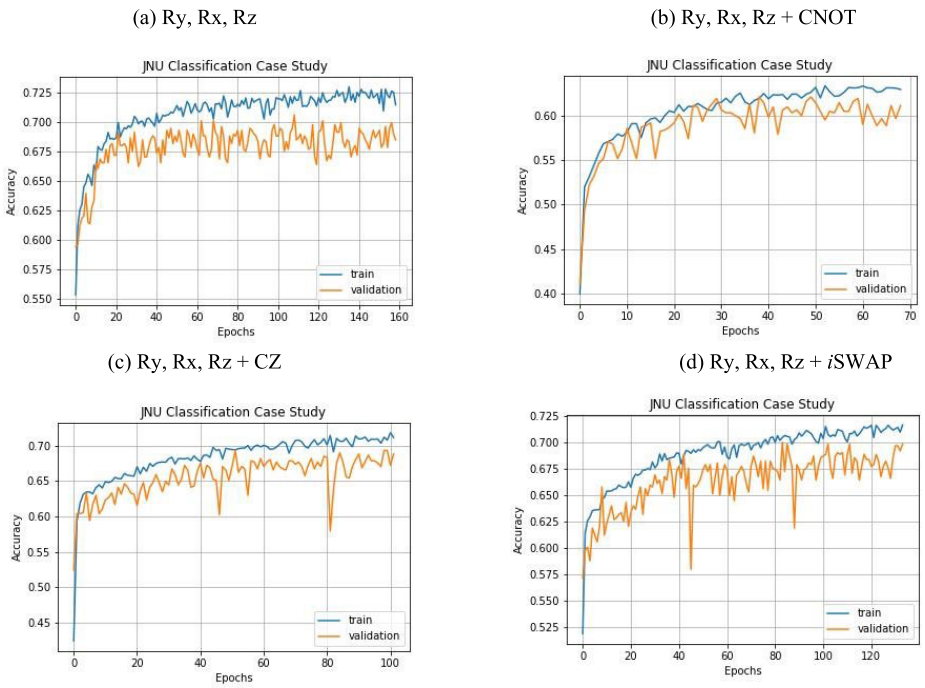

FIGURE 11. JNU accuracy curves for 1 layer PQCs for the following configurations: (a) Ry, Rx, Rz; (b) Ry, Rx, Rz + CNOT; (c) Ry, Rx, Rz + CZ; (d) Ry, Rx, Rz + iSWAP.

to be outstanding, and we can indicate it as the structure with entanglement presenting the worst performance for both databases.

Finally, it is possible to affirm that, when using the quantum simulator, there was no pattern regarding the increase in the number of layers and the improvement of the metrics. The results were generally better with up to five layers, decreasing when composing the circuit with ten layers. But there were cases where the inverse also happened.

Therefore, based on all findings, QML models outperformed MLP in the calculated metrics. However, many other ML model configurations could be compared. Furthermore, it is important to note that here we are not comparing QML with DL methods. Thus, in this study, it is not possible to judge whether the higher complexity DL algorithms are better than those of QML. Some studies in the literature apply DL methods that can achieve 100% accuracy, as in [11], but differently from our case, they use the full signal and have no input size limitations. We emphasize that the main focus is to show the applicability of these QML methods – on the rise in the literature [24], [28], [63] – in Reliability Engineering and to encourage their exploration in different machinery, sectors, and contexts that demand PHM activities, which are valuable to support maintenance decisions.

Finally, Table 8 shows the computational times, measured in seconds, required to train the models for the two databases (CWRU and JNU). The first point is that the classical MLP model achieves significantly less training time than the QML ones. The reason for this is that the models were trained on a simulator. Actual quantum hardware would likely achieve more agile times than those presented here.

When comparing the quantum models with each other, the fewer layers in the circuit, the faster the training becomes since the number of operations is smaller. It occurs in all scenarios.

TABLE 8. CWRU and JNU run times in seconds by model.

Category	Quantum gates	# of circuit layers	Run time (seconds)			
			CWRU		JNU	
			5 features	8 features	5 features	8 features
Classic ML (MLP)	-	-	3.00	1.30	7.30	7.41
QML	Ry, Rx, Rz	1	18.73	40.39	579.99	394.82
		5	36.30	74.44	751.31	1062.08
		10	86.31	168.38	875.50	3011.48
	VQE: Ry, Rx, Rz + CNOT	1	27.50	65.36	162.99	506.52
		5	51.11	128.81	1211.89	684.67
		10	75.43	220.98	2020.91	2583.07
	VQE: Ry, Rx, Rz + CZ	1	28.69	41.19	261.53	591.85
		5	70.47	173.35	555.65	2253.73
		10	121.43	505.76	1714.18	3612.71
	VQE: Ry, Rx, Rz + iSWAP	1	25.18	45.34	361.11	538.44
		5	68.56	90.58	1117.64	1378.35
		10	147.63	353.91	2526.39	2377.20

The training time of JNU is significantly longer than that of CWRU due to the complexity of the former. Lastly, we note that due to the early stopping inserted in training, some processes have more epochs than others, as presented in Fig. 11. Consequently, some training takes longer than others as well. Also, models with eight features, in most cases, have longer processing times than those with five features. That is, possibly the increase in the number of qubits also influences the longer processing time.''

VI. CONCLUSION

The main objective of this work was to develop a QML-based methodology for the PHM with applications to equipment through vibration signals. We bring results regarding bearing data available in the literature. The framework of QML models was based on an existing structure, but they have different combinations in the quantum part itself. That is, the proposed PQCs have other configurations in addition to rotation's gates. These are: the increment of the VQE algorithm combined with different two-qubit gates (CNOT, CZ and *i*SWAP). Moreover, additional layers of these circuits were used to identify if the increment of quantum operations, such as entanglement, would bring improvements in the results.

Regarding the CWRU, the model with CZ and 5 layers presented higher accuracy in the test data. Therefore, the effectiveness of a hybrid-quantum model for the diagnosis of failure modes for this type of equipment can be attested to in the scope of this study. Also, it was observed that when compared to the MLP model that has the same neural network configuration used for the quantum models, the QML results were better overall.

Concerning JNU, the best model in terms of accuracy was the VQE with CZ entanglement gates with 1 circuit layer. In this database, the model with the lowest accuracy was the MLP in both features configuration (5 and 8).

The contributions of this work are outlined in the following aspects: (1) exploration of two databases in the literature not yet analyzed in the QML framework; (2) performance of the diagnosis of a larger number of failure modes, compared to what has already been done in the literature; (3) delineation of the limitations of this study that can be a start kick for improvements and execution of new studies that cover the gaps of this one, as will be described throughout this conclusion; and, (4) to conduct a proof of concept that new quantum computing technologies can be used in Reliability Engineering problems, specifically in the diagnosis of failure modes of rotating machinery components, which are widely used in different sectors, such as in the O&G industry. Interested organizations may also be able to follow QC trends to modernize actions to help develop maintenance policies that are key points for the success of productive operations and safety.

It must be emphasized that, so far, there are many limitations in terms of the computational capacity of quantum programs. However, this is a promising path that tends to gain popularity in academia and companies. QC has received growing investments in terms of hardware in order to enable the resolution of problems with larger instances in a more efficient way.

Despite the promising results presented in this work, the QML models, given the framework we are using, are limited to the maximum number of qubits that the quantum library, Tensorflow quantum simulator, can handle. Thus, using a more extensive set of features is currently infeasible, and one must reduce the dimensionality to only a limited number of features, potentially losing information. Also, as we used simulators, we did not consider some real quantum hardware issues, such as the generated noises. Moreover, another limitation refers to the number of layers used in the circuit. Due to the computational capacity, applying more than 10 layers was not possible. We also observed that increasing the number of layers may enhance the QML models' performances due to increased quantum properties' effects, such as entanglement. However, not all tested QML models presented such a behavior.

The outcomes from this work support the notion that the proposed QML models constitute a promising strategy for handling features extracted from times series from multi-sensor suites for complex systems' health state diagnosis. The good performance of the models is competitive for reliability engineering studies, corroborating what was presented by Silva and Droguett [26]. Therefore, for future studies in this application area, it is suggested to explore different equipment besides rotating machines and analyze other stressors besides vibration, such as temperature. We also suggest the application of other configurations of quantum circuits, such as the QAOA and the combination of quantum circuits with other classical ML models. Additionally, another suggestion is to test different backpropagation methods besides the one used in this work, such as the parameter-shift rule. Finally, exploring different backpropagation methods in addition to the finite difference technique used in this work, such as the parameter-shift rule, could bring valuable insights.

COMPETING INTERESTS

The authors have declared that no competing interests exist.

REFERENCES

[1] E. Quatrini, F. Costantino, G. Di Gravio, and R. Patriarca, ''Condition-based maintenance—An extensive literature review,'' *Machines*, vol. 8, no. 2, p. 31, Jun. 2020.

[2] T. Zonta, C. A. da Costa, R. da Rosa Righi, M. J. de Lima, E. S. da Trindade, and G. P. Li, ''Predictive maintenance in the industry 4.0: A systematic literature review,'' *Comput. Ind. Eng.*, vol. 150, Dec. 2020, Art. no. 106889, doi: 10.1016/j.cie.2020.106889.

[3] J. F. Barraza, L. G. Bräuning, R. B. Perez, C. B. Morais, M. R. Martins, and E. L. Droguett, ''Deep learning health state prognostics of physical assets in the oil and gas industry,'' *Proc. Inst. Mech. Eng., O, J. Risk Rel.*, vol. 236, no. 4, pp. 598–616, Aug. 2022, doi: 10.1177/1748006X20976817.

[4] A. Kumar, R. Shankar, and L. S. Thakur, "A big data driven sustainable manufacturing framework for condition-based maintenance prediction," *J. Comput. Sci.*, vol. 27, pp. 428–439, Jul. 2018, doi: 10.1016/j.jocs.2017.06.006.

[5] C. B. S. Maior, M. D. C. Moura, I. D. Lins, E. L. Droguett, and H. H. L. Diniz, "Remaining useful life estimation by empirical mode decomposition and support vector machine," *IEEE Latin Amer. Trans.*, vol. 14, no. 11, pp. 4603–4610, Nov. 2016, doi: 10.1109/TLA.2016.7795836.

[6] P. F. Orrù, A. Zoccheddu, L. Sassu, C. Mattia, R. Cozza, and S. Arena, "Machine learning approach using MLP and SVM algorithms for the fault prediction of a centrifugal pump in the oil and gas industry," *Sustainability*, vol. 12, no. 11, p. 4776, Jun. 2020, doi: 10.3390/su12114776.

[7] S. B. Wang, X. F. Chen, C. W. Tong, and Z. B. Zhao, "Matching synchrosqueezing wavelet transform and application to aeroengine vibration monitoring," *IEEE Trans. Instrum. Meas.*, vol. 66, no. 2, pp. 360–372, Feb. 2016, doi: 10.1109/TIM.2016.2613359.

[8] S. Tang, C. Shen, D. Wang, S. Li, W. Huang, and Z. Zhu, "Adaptive deep feature learning network with Nesterov momentum and its application to rotating machinery fault diagnosis," *Neurocomputing*, vol. 305, pp. 1–14, Aug. 2018, doi: 10.1016/j.neucom.2018.04.048.

[9] Y. Zhang and K. Yang, "Fault diagnosis of submersible motor on offshore platform based on multi-signal fusion," *Energies*, vol. 15, no. 3, p. 756, Jan. 2022, doi: 10.3390/en15030756.

[10] L. Song, P. Chen, and H. Wang, "Vibration-based intelligent fault diagnosis for roller bearings in low-speed rotating machinery," *IEEE Trans. Instrum. Meas.*, vol. 67, no. 8, pp. 1887–1899, Aug. 2018, doi: 10.1109/TIM.2018.2806984.

[11] Z. Zhao, T. Li, J. Wu, C. Sun, S. Wang, R. Yan, and X. Chen, "Deep learning algorithms for rotating machinery intelligent diagnosis: An open source benchmark study," *ISA Trans.*, vol. 107, pp. 224–255, Dec. 2020, doi: 10.1016/j.isatra.2020.08.010.

[12] T. Lucas, L. Araújo, D. Aichele, M. C. Moura, and I. Lins, "Diagnosis of failure modes from bearing data via deep learning variational autoencoder method," in *Proc. Probabilistic Saf. Assessment Manag. (PSAM)*, 2022.

[13] C. B. S. Maior, M. C. Moura, and I. D. Lins, "Particle swarm-optimized support vector machines and pre-processing techniques for remaining useful life estimation of bearings," *Eksploatacja Niezawodnosc-Maintenance Rel.*, vol. 21, no. 4, pp. 610–619, 2019, doi: 10.17531/ein.2019.4.10.

[14] M. Hemmer, A. Klausen, H. V. Khang, K. G. Robbersmyr, and T. I. Waag, "Health indicator for low-speed axial bearings using variational autoencoders," *IEEE Access*, vol. 8, pp. 35842–35852, 2020.

[15] J. Xie, G. Du, C. Shen, N. Chen, L. Chen, and Z. Zhu, "An end-to-end model based on improved adaptive deep belief network and its application to bearing fault diagnosis," *IEEE Access*, vol. 6, pp. 63584–63596, 2018, doi: 10.1109/ACCESS.2018.2877447.

[16] S. S. Afshari, F. Enayatollahi, X. Xu, and X. Liang, "Machine learning-based methods in structural reliability analysis: A review," *Rel. Eng. Syst. Saf.*, vol. 219, Mar. 2022, Art. no. 108223, doi: 10.1016/j.ress.2021.108223.

[17] C. Ferreira and G. Gonçalves, "Remaining useful life prediction and challenges: A literature review on the use of machine learning methods," *J. Manuf. Syst.*, vol. 63, pp. 550–562, Apr. 2022, doi: 10.1016/j.jmsy.2022.05.010.

[18] Y. Liu, H. Jiang, Y. Wang, Z. Wu, and S. Liu, "A conditional variational autoencoding generative adversarial networks with self-modulation for rolling bearing fault diagnosis," *Measurement*, vol. 192, Mar. 2022, Art. no. 110888, doi: 10.1016/j.measurement.2022.110888.

[19] S. J. Nawaz, S. K. Sharma, S. Wyne, M. N. Patwary, and M. Asaduzzaman, "Quantum machine learning for 6G communication networks: State-of-the-art and vision for the future," *IEEE Access*, vol. 7, pp. 46317–46350, 2019, doi: 10.1109/ACCESS.2019.2909490.

[20] A. W. Harrow and A. Montanaro, "Quantum computational supremacy," *Nature*, vol. 549, no. 7671, pp. 203–209, Sep. 2017, doi: 10.1038/nature23458.

[21] S. S. Kavitha and N. Kaulgud, "Quantum machine learning for support vector machine classification," *Evol. Intell.*, vol. 2022, pp. 1–10, Jul. 2022, doi: 10.1007/s12065-022-00756-5.

[22] D. Sierra-Sosa, M. Telahun, and A. Elmaghraby, "TensorFlow quantum: Impacts of quantum state preparation on quantum machine learning performance," *IEEE Access*, vol. 8, pp. 215246–215255, 2020, doi: 10.1109/ACCESS.2020.3040798.

[23] T. M. Khan and A. Robles-Kelly, "Machine learning: Quantum vs classical," *IEEE Access*, vol. 8, pp. 219275–219294, 2020, doi: 10.1109/ACCESS.2020.3041719.

[24] J. Biamonte, P. Wittek, N. Pancotti, P. Rebentrost, N. Wiebe, and S. Lloyd, "Quantum machine learning," *Nature*, vol. 549, pp. 195–202, Sep. 2017, doi: 10.1038/nature23474.

[25] D. P. García, J. Cruz-Benito, and F. José García-Peñalvo, "Systematic literature review: Quantum machine learning and its applications," 2022, *arXiv:2201.04093*.

[26] G. S. M. Silva and E. L. Droguett, "Quantum machine learning for health state diagnosis and prognostics," in *Proc. Annu. Rel. Maintainability Symp. (RAMS)*, Jan. 2022, pp. 1–7, doi: 10.1109/RAMS51457.2022.9893971.

[27] C. Correa-Jullian, S. Cofre-Martel, G. S. Martin, E. L. Droguett, G. N. P. de Leite, and A. Costa, "Exploring quantum machine learning and feature reduction techniques for wind turbine pitch fault detection," *Energies*, vol. 15, no. 8, pp. 1–29, 2022, doi: 10.3390/en15082792.

[28] A. Perdomo-Ortiz, M. Benedetti, J. Realpe-Gómez, and R. Biswas, "Opportunities and challenges for quantum-assisted machine learning in near-term quantum computers," *Quantum Sci. Technol.*, vol. 3, no. 3, Jun. 2018, Art. no. 030502, doi: 10.1088/2058-9565/aab859.

[29] L. M. M. Araújo, I. D. Lins, D. A. A. Figueroa, C. B. S. Maior, M. C. Moura, and E. L. Droguett, "Review of quantum (-inspired) optimization methods for system reliability problems," in *Proc. Probabilistic Saf. Assessment Manag. (PSAM)*, 2022.

[30] A. Ajagekar and F. You, "Quantum computing for energy systems optimization: Challenges and opportunities," *Energy*, vol. 179, pp. 76–89, Jul. 2019, doi: 10.1016/j.energy.2019.04.186.

[31] A. M. Khalaf and A. C. Seibi, "Failure analysis of lube oil feed tube of a gas turbine operating in oil fields," *Eng. Failure Anal.*, vol. 18, no. 5, pp. 1341–1350, Jul. 2011, doi: 10.1016/j.engfailanal.2011.03.023.

[32] CWRU. (2020). *Case Western Reserve University Bearing Data Center Website*. Accessed: Jun. 22, 2023. [Online]. Available: https://csegroups.case.edu/bearingdatacenter/pages/welcome-case-western-reserve-university-bearing-data-center-website

[33] JNU. (2019). *JNU Dataset*. Jiangnan University. Accessed: Jan. 22, 2023. [Online]. Available: http://mad-net.org:8765/explore.html?t=0.5831516555847212

[34] Y. Wang and H. Liu, "Quantum computing in a statistical context," *Annu. Rev. Statist. Appl.*, vol. 9, no. 1, pp. 479–504, Mar. 2022, doi: 10.1146/annurev-statistics-042720-024040.

[35] M. Schönberger, "Applicability of quantum computing on database query optimization," in *Proc. Int. Conf. Manage. Data*, 2022, pp. 2512–2514, doi: 10.1145/3514221.3520257.

[36] A. Montanaro, "Quantum algorithms: An overview," *NPJ Quantum Inf.*, vol. 2, no. 1, pp. 1–8, Jan. 2016, doi: 10.1038/npjqi.2015.23.

[37] S. E. Rasmussen and N. T. Zinner, "Parameterized two-qubit gates for enhanced variational quantum eigensolver," *Annalen Physik*, vol. 534, no. 12, Dec. 2022, Art. no. 2200338, doi: 10.1002/andp.202200338.

[38] Y. Li, R.-G. Zhou, R. Xu, J. Luo, and S.-X. Jiang, "A quantum mechanics-based framework for EEG signal feature extraction and classification," *IEEE Trans. Emerg. Topics Comput.*, vol. 10, no. 1, pp. 211–222, Jan. 2022, doi: 10.1109/TETC.2020.3000734.

[39] S. Yarkoni, E. Raponi, T. Bäck, and S. Schmitt, "Quantum annealing for industry applications: Introduction and review," *Rep. Prog. Phys.*, vol. 85, no. 10, Oct. 2022, Art. no. 104001.

[40] J. Tilly, H. Chen, S. Cao, D. Picozzi, K. Setia, Y. Li, E. Grant, L. Wossnig, I. Rungger, G. H. Booth, and J. Tennyson, "The variational quantum eigensolver: A review of methods and best practices," *Phys. Rep.*, vol. 986, pp. 1–128, Nov. 2022, doi: 10.1016/j.physrep.2022.08.003.

[41] S. Sim, P. D. Johnson, and A. Aspuru-Guzik, "Expressibility and entangling capability of parameterized quantum circuits for hybrid quantum-classical algorithms," *Adv. Quantum Technol.*, vol. 2, no. 12, Dec. 2019, Art. no. 1900070, doi: 10.1002/qute.201900070.

[42] M. Schuld and F. Petruccione, *Supervised Learning With Quantum Computers*, 1st ed. New York, NY, USA: Springer, 2018, doi: 10.1007/978-3-319-96424-9.

[43] K. B. Prakash, "Quantum meta-heuristics and applications," in *Cognitive Engineering for Next Generation Computing: A Practical Analytical Approach*, 1st ed. Beverly, MA, USA: Scrivener Publishing, 2021, pp. 265–297.

[44] E. Osaba, E. Villar-Rodriguez, I. Oregi, and A. Moreno-Fernandez-de-Leceta, "Hybrid quantum computing—Tabu search algorithm for partitioning problems: Preliminary study on the traveling salesman problem," in *Proc. IEEE Congr. Evol. Comput. (CEC)*, Jun. 2021, pp. 351–358, doi: 10.1109/CEC45853.2021.9504923.
[45] O. H. M. Ross, "A review of quantum-inspired metaheuristics: Going from classical computers to real quantum computers," *IEEE Access*, vol. 8, pp. 814–838, 2020, doi: 10.1109/ACCESS.2019.2962155.
[46] H.-P. Chiang, Y.-H. Chou, C.-H. Chiu, S.-Y. Kuo, and Y.-M. Huang, "A quantum-inspired Tabu search algorithm for solving combinatorial optimization problems," *Soft Comput.*, vol. 18, no. 9, pp. 1771–1781, 2014, doi: 10.1007/s00500-013-1203-7.
[47] W. Scherer, *Mathematics of Quantum Computing*. Cham, Switzerland: Springer, 2019, doi: 10.1007/978-3-030-12358-1.
[48] M. Nielsen and I. Chuang, "Quantum computation and quantum information," *Phys. Today*, vol. 54, no. 2, p. 60, 2010, doi: 10.1080/00107514.2011.587535.
[49] H. Shareef, A. A. Ibrahim, N. Salman, A. Mohamed, and W. L. Ai, "Power quality and reliability enhancement in distribution systems via optimum network reconfiguration by using quantum firefly algorithm," *Int. J. Electr. Power Energy Syst.*, vol. 58, pp. 160–169, Jun. 2014, doi: 10.1016/j.ijepes.2014.01.013.
[50] D. Konar, S. Bhattacharyya, K. Sharma, S. Sharma, and S. R. Pradhan, "An improved hybrid quantum-inspired genetic algorithm (HQIGA) for scheduling of real-time task in multiprocessor system," *Appl. Soft Comput.*, vol. 53, pp. 296–307, Apr. 2017, doi: 10.1016/j.asoc.2016.12.051.
[51] Z. Ke, C. Di, and X. Bao, "Adaptive suppression of mode mixing in CEEMD based on genetic algorithm for motor bearing fault diagnosis," *IEEE Trans. Magn.*, vol. 58, no. 2, pp. 1–6, Feb. 2022, doi: 10.1109/TMAG.2021.3082138.
[52] Z. Ye and J. Yu, "Deep morphological convolutional network for feature learning of vibration signals and its applications to gearbox fault diagnosis," *Mech. Syst. Signal Process.*, vol. 161, Dec. 2021, Art. no. 107984, doi: 10.1016/j.ymssp.2021.107984.
[53] K. Li, X. Ping, H. Wang, P. Chen, and Y. Cao, "Sequential fuzzy diagnosis method for motor roller bearing in variable operating conditions based on vibration analysis," *Sensors*, vol. 13, pp. 8013–8041, May 2013, doi: 10.3390/s130608013.
[54] R. S. Peruchi, P. R. Junior, T. G. Brito, A. P. Paiva, P. P. Balestrassi, and L. M. Mendes Araujo, "Integrating multivariate statistical analysis into six sigma DMAIC projects: A case study on AISI 52100 hardened steel turning," *IEEE Access*, vol. 8, pp. 34246–34255, 2020, doi: 10.1109/ACCESS.2020.2973172.
[55] L. M. M. Araújo, R. G. N. Paiva, R. S. Peruchi, P. R. Junior, and J. H. de Freitas Gomes, "New indicators for measurement error detection in GR&R studies," *Measurement*, vol. 140, pp. 557–564, Jul. 2019, doi: 10.1016/j.measurement.2019.03.059.
[56] B. R. Nayana and P. Geethanjali, "Analysis of statistical time-domain features effectiveness in identification of bearing faults from vibration signal," *IEEE Sensors J.*, vol. 17, no. 17, pp. 5618–5625, Sep. 2017.
[57] N. Lybeck, S. Marble, and B. Morton, "Validating prognostic algorithms: A case study using comprehensive bearing fault data," in *Proc. IEEE Aerosp. Conf.*, Mar. 2007, pp. 1–9, doi: 10.1109/AERO.2007.352842.
[58] Y. Kim, J. Park, K. Na, H. Yuan, B. D. Youn, and C.-S. Kang, "Phase-based time domain averaging (PTDA) for fault detection of a gearbox in an industrial robot using vibration signals," *Mech. Syst. Signal Process.*, vol. 138, Apr. 2020, Art. no. 106544.
[59] B. Roser, A. Jaume, A. Rafael, and B. J. Maria, "Bias, precision, and accuracy of skewness and kurtosis estimators for frequently used continuous distributions," *Symmetry*, vol. 12, no. 19, pp. 2–17, 2020.
[60] J. Antoni and P. Borghesani, "A statistical methodology for the design of condition indicators," *Mech. Syst. Signal Process.*, vol. 114, pp. 290–327, Jan. 2019, doi: 10.1016/j.ymssp.2018.05.012.
[61] Y. Li, M. J. Zuo, Y. Chen, and K. Feng, "An enhanced morphology gradient product filter for bearing fault detection," *Mech. Syst. Signal Process.*, vol. 109, pp. 166–184, Sep. 2018, doi: 10.1016/j.ymssp.2018.03.002.
[62] F. Hemmati, W. Orfali, and M. S. Gadala, "Roller bearing acoustic signature extraction by wavelet packet transform, applications in fault detection and size estimation," *Appl. Acoust.*, vol. 104, pp. 101–118, Mar. 2016.
[63] M. Broughton et al., "TensorFlow quantum: A software framework for quantum machine learning," 2020, *arXiv:2003.02989*.

CAIO BEZERRA SOUTO MAIOR received the bachelor's, master's, and Ph.D. degrees in production engineering from the Federal University of Pernambuco (UFPE), in 2015, 2017, and 2020, respectively. He was a Visiting Scholar with The B. John Garrick Institute for the Risk Sciences, University of California, Los Angeles (UCLA), in 2022, a Postdoctoral Researcher with the Graduate Program in Production Engineering, UFPE (PPGEP), from 2020 to 2021, and a Sandwich Graduate Student in the industrial organization with the Polytechnic University of Catalonia (UPC), Catalonia, Spain, from 2012 to 2013. He is currently an Assistant Professor with the Technology Center (NT), Federal University of Pernambuco (UFPE), and a Researcher with the Center for Risk Analysis, Reliability Engineering and Environmental Modeling (CEERMA-UFPE). His research interests include reliability engineering, machine learning (quantum, deep, machine), computer vision, signal analysis, and risk analysis. He is a member of the Brazilian Association for Risk Analysis, Process Safety and Reliability (ABRISCO) and a permanent member of PPGEP, NT (PPGEP-CAA). He is a Regular Reviewer of journals, such as *Reliability Engineering and Systems Safety*, IEEE TRANSACTIONS ON INSTRUMENTATION AND MEASUREMENT, IEEE ACCESS, and *Safety Science*.

LAVÍNIA MARIA MENDES ARAÚJO received the degree in production engineering from Universidade Federal da Paraíba (UFPB), in 2020, with a one-year exchange at École Génie Industriel-Grenoble INP/Grenoble, France, from 2019 to 2020, and the M.Sc. degree in production engineering from Universidade Federal de Pernambuco (UFPE), in 2023, where she is currently pursuing the Ph.D. degree in production engineering. She is a scholarship holder of the human resources program of the National Petroleum Agency (ANP)–PRH 38.1 and a member of the Center for Risk Analysis, Reliability Engineering and Environmental Modeling (CEERMA/UFPE). Her research interests include reliability engineering, optimization, quantum computing, and deep and machine learning.

ISIS DIDIER LINS received the B.S., M.Sc., and D.Sc. degrees in production engineering, with a focus on operational research, from Universidade Federal de Pernambuco (UFPE), Recife, Brazil, in 2007, 2010, and 2013, respectively. She is currently an Assistant Professor with the Department of Production Engineering and a Researcher with the Center for Risk Analysis, Reliability Engineering and Environmental Modeling (CEERMA), UFPE. Her research interests include investigating and adapting machine learning and optimization methods, including their quantum versions, to be applied in the context of risk and reliability, specifically in the prognostics and health management (PHM) of technical systems. She was a recipient of the CAPES Thesis Award 2014–Engineering III from the Coordination for the Improvement of Higher Education Personnel (CAPES). She has been receiving a research productivity scholarship from the National Council for Scientific and Technological Development (CNPq), since 2016.

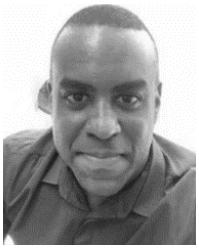

MÁRCIO DAS CHAGAS MOURA received the Ph.D. degree in reliability engineering from Universidade Federal de Pernambuco (UFPE), in 2009. He is currently a Research Leader with the Center for Risk Analysis, Reliability Engineering and Environmental Modeling (CEERMA) and is a permanent member of the Graduate Program in Production Engineering. He is also an Associate Professor with the Technology and Geoscience Centre, Department of Production Engineering, UFPE, where he teaches courses for undergraduate and post-graduate students. Since 2014, he has been a Coordinator of the Human Resources Training Program managed by the Brazilian Petroleum Agency, whose emphasis is ''Sustainability Management for Exploration and Production of Petroleum in the Equatorial Band.'' Yet, he has been actively involved in joint research projects with companies in the energy sector. His research interests include reliability engineering, risk assessment, and simulation and optimization of production processes. He has been a Regular Reviewer of the journals *Reliability Engineering and System Safety*, *Journal of Risk and Reliability*, and *Quality Engineering and Reliability International*.

ENRIQUE LÓPEZ DROGUETT is currently a Professor with the Department of Civil and Environmental Engineering and The B. John Garrick Institute for the Risk Sciences, University of California, Los Angeles (UCLA), USA. He researches Bayesian inference and artificial intelligence, supported digital twins and prognostics, and health management based on physics-informed deep learning for reliability, risk, and safety assessment of structural and mechanical systems. His most recent focus has been on quantum computing and quantum machine learning for developing solutions for risk and reliability quantification and energy efficiency of complex systems, particularly those involved in renewable energy production. He has led many major studies on these topics for a broad range of industries, including oil and gas, nuclear energy, defense, civil aviation, mining, renewable and hydro energy production, and distribution networks. He has authored more than 300 papers in archival journals and conference proceedings. He is an Associate Editor of the *Journal of Risk and Reliability* and the *International Journal of Reliability and Safety*. He also serves on the Board of Directors of the International Association for Probabilistic Safety Assessment and Management (IAPSAM).